International Journal for Multiscale Computational Engineering, 18(1):1–30 (2020)

COMPUTATIONAL APPLICATIONS IN MASONRY STRUCTURES: FROM THE MESO-SCALE TO THE SUPER-LARGE/SUPER-COMPLEX

Paulo B. Lourenço & Luís C. Silva*

Deptartment of Civil Engineering, ISISE, University of Minho, Azurém, 4800-058 Guimarães, Portugal

*Address all correspondence to: Luís C. Silva, Deptartment of Civil Engineering, ISISE, University of Minho, Azurém, 4800-058 Guimarães, Portugal, E-mail: luisilva.civil@gmail.com

Original Manuscript Submitted: 4/30/2019; Final Draft Received: 9/3/2019

Masonry structures constitute a large portion of the built heritage around the world, from the past until today. Therefore, understanding their structural behavior is crucial for preserving the historical characteristics of many buildings and in addressing the requirements for housing and sustainable development. Due to its composite and highly nonlinear nature, the analysis of masonry structures has been a challenge for engineers.

This article presents a set of advanced models for the mechanical study of masonry, including the usual micro-modeling approaches (the masonry constituents, unit and joint, are represented separately), macro-modeling (masonry constituents are smeared in a homogeneous composite), and multi-scale techniques (upscaling from micro to macro is adopted). An extensive overview of its computational features is provided. The engineering application of such strategies is presented and covers problems from the masonry components level (meso-scale) to the structural element itself, and ultimately to the level of monumental buildings (super-large). The structural safety assessment and/or strengthening schemes evaluation are performed amid the static, slow dynamics or earthquakes, and fast dynamics or impact and blast ranges.

KEY WORDS: *masonry, micro-modeling, macro-modeling, multi-scale, homogenization, URM applications, seismic load, fast dynamics, out-of-plane*

1. INTRODUCTION

Masonry is an ancient but still widely used material. Its usage has been mainly fostered by the simplicity of this type of construction, where masonry units are laid together with or without the use of bonding mortar. Features such as its durability, aesthetics, low maintenance, adaptability, good sound, and thermal insulation properties (Hendry, 2001) are also important for allowing continuous applications for masonry. Unreinforced masonry (URM) buildings are a relevant part of the worldwide building stock. These include stone, brick, adobe, or earthen masonry structures and represent, in countries such as Mexico, Pakistan, and Peru, more than 75% over its total buildings' inventory. In other countries (Iran, Australia, Indonesia, or Italy), the relative percentage is higher than 50% (Frankie et al., 2013). A similar trend is found in Portugal, with a value of about 50%, according to the Portuguese Census of Population and Housing.

Most of this widespread built heritage has been achieved based on empirical knowledge passed by generation to generation and, therefore, the structural behavior of URM was often ill-understood. These constructions have been typically made to withstand vertical loads, and its low strength/mass ratio makes the buildings rather vulnerable to dynamic horizontal loads as earthquakes, impact, or blast actions. This addresses the importance of carrying out urgent measures in the URM built stock to avoid human and societal consequences and to minimize future economic impacts. Yet, intervening in these constructions is a complex process, due to the lack of structural information and

1543–1649/20/$35.00

due to their high importance. A scientifically-based process is less susceptible to inadequate actions, which clearly sets a convenient context for the continuous development of numerical strategies.

Advanced computational strategies have been developed in the last few decades. Conversely to concrete and steel structures, the design guidelines for masonry did not go always hand in hand with the application of innovative methods. Still, it is currently well accepted that sophisticated strategies, mainly based on the finite element (FE) method, constitute important tools that deserve more attention from the scientific community. Three main modeling strategies for the mechanical study of masonry are: (i) direct numerical simulation or micro-modeling approaches [masonry constituents, (unit and joint) are represented separately]; (ii) macro-modeling (masonry constituents are smeared in a homogeneous composite); and (iii) the multi-scale techniques (upscaling from the meso-scale to the macro-scale is adopted). The mechanical complexity of masonry may demand, in some cases, more detailed analysis with a focus on the component levels. Although accurate, a direct numerical simulation (micro-modeling) is expensive to carry out from a computational standpoint and, therefore, macro- or multi-scale techniques can be more appropriate for large or super-large problems. An engineering compromise between the solution accuracy and the time-cost demand needs to be assumed which, depending on the nature of the problem, may constitute a real challenge.

2. GENERAL SCOPE

Prevailing design rules or analytical approaches still are, within engineering practice, the most useful in the structural analysis of URM buildings. These pose, however, several well-identified limitations that may lead to potential unrealistic or conservative results (Theodossopoulos and Sinha, 2013). Other simplified procedures, as the story-mechanism (Tomaževič, 1999) and the equivalent frame-based models (Lagomarsino et al., 2013; Quagliarini and Maracchini, 2017) can also be found in the literature. Such models, however, hardly consider the out-of-plane failure modes and thus these are generally disregarded in most study cases. More suitable and yet conceptually simple procedures, as the rigid-body approaches (Konstantinidis and Makris, 2007; D'Ayala and Shi, 2011) or the well disseminated kinematic methods (D'Ayala and Speranza, 2003; Griffith and Magenes, 2003; Calvi et al., 2006), are useful to provide closed-form solutions under dynamic excitations but are very complex for walls subjected to two-way bending.

Sophisticated FE computational strategies deserve more attention from the scientific community. Several advances have been achieved in the last few decades and these constitute important (sometimes indispensable) analysis tools. For the masonry field, it is recognizable that two scale levels are of interest when analyzing structural behavior (Lourenço, 2009; Roca et al., 2010), the macro- and the meso-scales (Fig. 1). Again, three main modeling strategies can be put together, namely (i) the direct simulation or the micro-modeling; (ii) macro-modeling; and (iii) multi-scale modeling.

In the micro-modeling approach, both masonry components (units and mortar joints) are explicitly represented. These are certainly capable of well reproducing both in- and out-of-plane orthotropic nonlinear behavior of masonry

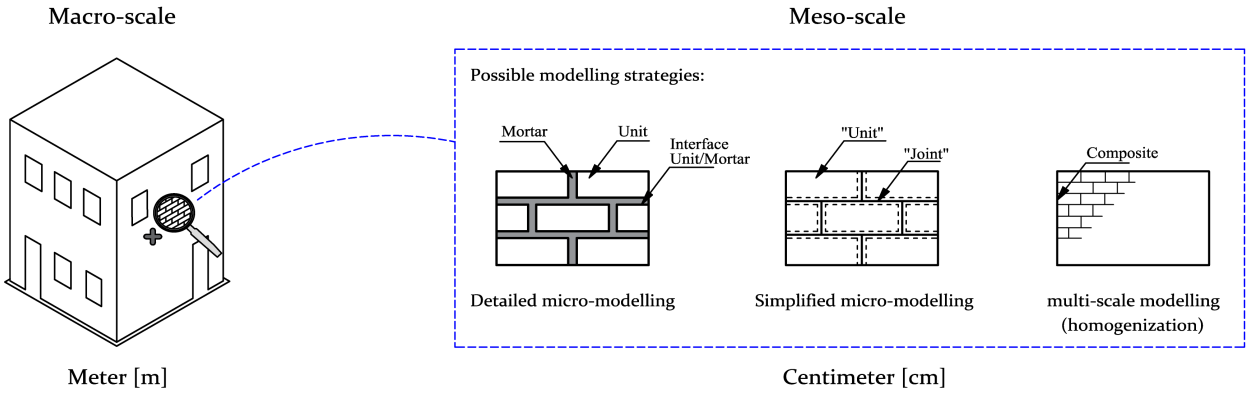

FIG. 1: Representation of the three scales considered in the analysis of masonry for this study: macro-scale and meso-scale. Definition of the modeling strategies adopted to represent masonry.

but are characterized by long processing times, being only recommended for limited size structural problems (Lotfi and Shing, 1994; Giambanco and Rizzo, 2001; Lemos, 2007; Sejnoha et al., 2008; Adam et al., 2010; Macorini and Izzuddin, 2011, 2013; Sarhosis et al., 2014). The macro-modeling strategies smear out the heterogeneous assemblage of mortar and bricks into a fictitious homogeneous anisotropic material. The use of closed-form laws to represent the complex phenomenological behavior and damage of the masonry may be cumbersome, as it may require a calibration step (usually achieved by thorough experimental campaigns). However, this approach allows studying large-scale structures without the drawbacks exhibited by meso-modeling (Dhanasekar et al., 1985; Lourenço et al., 1997; Berto et al., 2002; Roca et al., 2013).

Multi-scale FE (or FE^2) methods are in-between the latter two FE modeling schemes. The framework is being used to investigate the response of composites with different natures (Spahn et al., 2014; Trovalusci et al., 2015; Greco et al., 2017; Leonetti et al., 2018). It typically relies on a meso- and macro-transition of information and is, therefore, designated as two-scale or FE^2 approaches. Full continuum-based FE^2 approaches result in a good compromise between solution accuracy and computational cost. Nevertheless, these methods still constitute a challenge if one desires to account for the material nonlinearity (Geers et al., 2010; Otero et al., 2015). In fact, the constant need of data between the macro- and meso- scales constitute a contentious issue, because a new boundary value problem (BVP) must be solved numerically for each load step and in each Gauss integration point. The utility of the approach is compromised due to the involved computational time, and thus full continuum-based FE^2 approaches are seldom used for dynamic purposes or for complex structural analysis. An adequate possibility is the use of a two-scale simplified strategy, for instance, by using a kinematic theorem of limit analysis at a macro-level to obtain the homogenized failure surfaces with a very limited computational effort (de Buhan and de Felice, 1997; Milani et al., 2006; Cecchi and Milani, 2008). Yet, the use of discrete FE-based methods at a macro-level seems to be a promising alternative (Silva et al., 2017b; Casolo and Milani, 2010; Milani and Tralli, 2011).

In this context, three advanced FE-based models, for which the authors gave their contribution, are hereafter addressed and each one belongs to one of the aforementioned modeling strategies (Fig. 1): a simplified micro-model; a macro-model; and a simplified two-scale (FE^2) model. Note that the strategies can handle the masonry full softening behavior, anisotropy, and its strain-rate dependency under fast dynamic cases. Furthermore, all the strategies have been implemented in advanced FE softwares.

3. PROPOSED MODELING STRATEGIES

3.1 FE Mesoscopic Model

An FE mesoscopic model first introduced by Lourenço (1996) within the so-called simplified micro-modeling approach is presented next. The interface model for masonry has the ability to reproduce the loading strain-rate effects on the material properties (Rafsanjani et al., 2015b). A multi-surface plasticity model, the so-called composite interface model, is typically considered for the mortar joints and is suitable to reproduce fracture, frictional slip, and crushing along the interface elements.

The assumption that all the inelastic phenomena occur in the interface elements leads to a robust type of modeling, which can follow the complete load path of a structure until the total degradation of stiffness. For a 3D configuration, the linear elastic relation between the generalized stresses and strains of the interface FE is given by $\boldsymbol{\sigma} = \boldsymbol{D}\boldsymbol{\varepsilon}$, whereas the stiffness matrix is $\boldsymbol{D} = \mathrm{diag}\{k_n, k_s, k_t\}$ (the subscript n refers to the normal and the subscripts s and t to the shear components).

The constitutive interface model is defined by a convex composite yield criterion with three individual functions, specifically: (i) a tension cut-off criterion designated as $f_{\mathrm{criterion},1}$ and defined in Eq. (1); (ii) a Mohr–Coulomb shear criterion designated as $f_{\mathrm{criterion},2}$ and defined in Eq. (2); and (iii) a cap in compression designated as $f_{\mathrm{criterion},3}$ and defined in Eq. (3). Softening behavior is represented in all the modes. The tensile criterion [Fig. 2(a)] reads:

$$f_{\mathrm{criterion},1}(\sigma, \kappa_1) = \sigma - \bar{\sigma}_1(\kappa_1) \;\text{ and }\; \bar{\sigma}_1 = f_t \exp\left(-\frac{f_t}{G_f^I}\kappa_1\right) \tag{1}$$

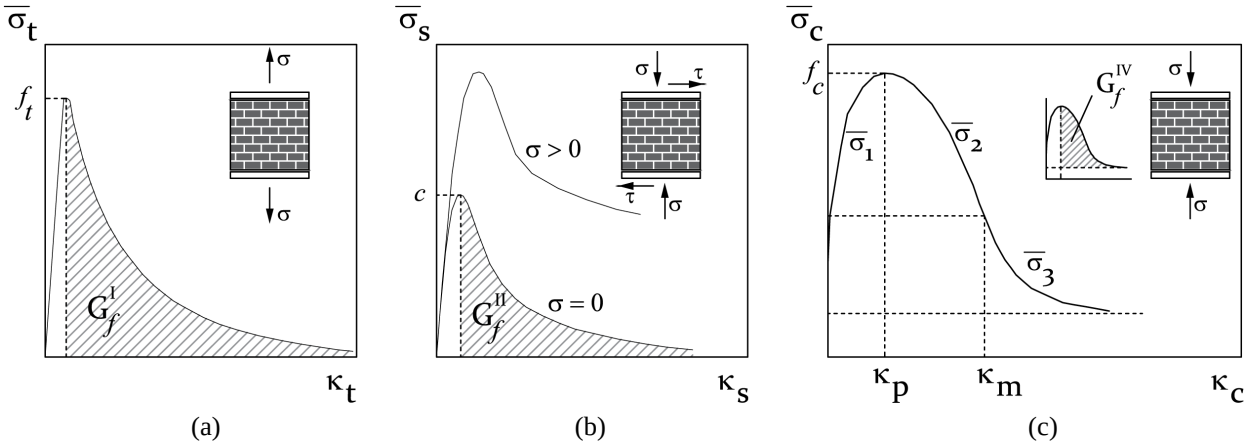

FIG. 2: Multi-surface plasticity model adopted for the mortar joints (interface FEs). The behavior of quasi-brittle materials under (a) tensile loading (mode-I, f_t is the tensile strength); (b) shear loading (mode-II, c is the cohesion) accounting with a potential pre-compression level; (c) compressive load (f_c is the compressive strength; p and m are the peak and medium values, respectively).

The shear criterion [Fig. 2(b)] is given as:

$$f_{\text{criterion},2}(\boldsymbol{\sigma}, \kappa_2) = |\tau| + \sigma \tan\phi(\kappa_2) - \bar{\sigma}_2(\kappa_2) \;\text{ and }\; \bar{\sigma}_2 = c \exp\left(-\frac{c}{G_f^{II}}\kappa_2\right) \tag{2}$$

For the compressive yield function [Fig. 2(c)] and using a matrix form:

$$f_{\text{criterion},3}(\boldsymbol{\sigma}, \kappa_2) = 1/2\left(\boldsymbol{\sigma}^T \boldsymbol{P} \boldsymbol{\sigma}\right) + \boldsymbol{p}^T \boldsymbol{\sigma} - \bar{\sigma}_3^2(\kappa_3) \tag{3}$$

Here, $\boldsymbol{\sigma}$ is the generalized stresses, f_t is the interface bond strength, c is the interface cohesion strength, ϕ is the friction angle; $\boldsymbol{P}$ is a projection diagonal matrix and $\boldsymbol{p}$ a projection vector based on material parameters; G_f^I, G_f^{II} are the mode-I and mode-II fracture energy terms, respectively; $\bar{\sigma}_1$, $\bar{\sigma}_2$, and $\bar{\sigma}_3$ are the effective stresses of each adopted yield functions governed by the internal scalar variables κ_1, κ_2, and κ_3, respectively. Note that the typical compressive hardening/softening law $\bar{\sigma}_3(\kappa_3)$ is composed of three branches, as observed in Fig. 2(c), which are in agreement with the $\bar{\sigma}_{c1}(\kappa_3)$, $\bar{\sigma}_{c2}(\kappa_3)$, and $\bar{\sigma}_{c3}(\kappa_3)$ laws defined by Lourenço and Rots (1997), and presented in Eq. (4). Note that the subscripts i, m, and r for both the yield stress value and scalar κ indicates the initial, medium, and residual values, respectively. The compressive fracture energy G_f^{IV} depicted in Fig. 2(c) corresponds to a material input parameter of the model and allows computing the residual strength value $\bar{\sigma}_r$ (from the peak $\bar{\sigma}_p$ one).

$$\bar{\sigma}_{c1}(\kappa_3) = \bar{\sigma}_i + (\bar{\sigma}_p - \bar{\sigma}_i)\sqrt{\frac{2\kappa_3}{\kappa_p} - \frac{\kappa_3^2}{\kappa_p^2}} \tag{4a}$$

$$\bar{\sigma}_{c2}(\kappa_3) = \bar{\sigma}_p + (\bar{\sigma}_m - \bar{\sigma}_p)\left(\frac{\kappa_3 - \kappa_p}{\kappa_m - \kappa_p}\right)^2 \tag{4b}$$

$$\bar{\sigma}_{c3}(\kappa_3) = \bar{\sigma}_r + (\bar{\sigma}_m - \bar{\sigma}_p)\exp\left(m\frac{\kappa_3 - \kappa_m}{\bar{\sigma}_m - \bar{\sigma}_r}\right)^2, \quad m = 2\frac{\bar{\sigma}_m - \bar{\sigma}_p}{\kappa_m - \kappa_p} \tag{4c}$$

It may be highlighted that a penalty approach is not followed by the adopted interface FEs to phenomenologically represent the behavior of masonry crushing. Here, penetration and overlapping between neighboring brick units can occur which does not blur the adequacy of the strategy. The dynamic interface model has been implemented in

the software DIANA (2017) (strain-rate independent) and in ABAQUS (2013) (strain-rate dependent). In the latter, a FORTRAN user-subroutine was developed, and the material model is introduced by a failure criterion. A Euler backward algorithm (linear predictor-plastic corrector approach) is adopted for the stress update process. The user-subroutine VUINTER provided in ABAQUS is involved to define contact interface behavior. The interface material is assumed to be bonded to each of two contacting surfaces (slave and master surfaces) and, again, the material strength values are sensitive to the load strain-rate level [see Lourenço and Rots (1997) and Rafsanjani et al. (2015b), for further details].

3.2 FE Macroscopic Model

Several continuum models have been presented in the literature, albeit especially indicated for concrete-like materials, such as the well-known 'Barcelona' model by Lubliner et al. (1989), the 'Microplane' model (Bažant et al., 1996), the Concrete Damage Plasticity (CDP) model (Lee and Fenves, 1998), and the Pontiroli, Rouquard, and Mazars (PRM) model presented in Pontiroli et al. (2010). Here, a plasticity continuum model is presented for the static and dynamic study of masonry. The model stems from the anisotropic continuum model for masonry shells and plates proposed by Lourenço (1997, 2000), in which the so-called composite yield criterion is defined. The formulation is briefly recalled here for a 3D stress space, whereas the stress and strain tensors are typically represented as six-components vectors owing the symmetry conditions, and given as follows:

$$\boldsymbol{\sigma} = \{\sigma_x, \sigma_y, \sigma_z, \tau_{xy}, \tau_{yz}, \tau_{xz}\}^T$$

$$\boldsymbol{\varepsilon} = \{\varepsilon_x, \varepsilon_y, \varepsilon_z, \gamma_{xy}, \gamma_{yz}, \gamma_{xz}\}^T$$

The anisotropy of the material behavior is considered since different hardening/softening regimes can be introduced for different axes. The so-called composite yield surface (Lourenço, 1997) is adopted and, therefore, a total of three Rankine-type yield criterion are defined in tension and a Hill-type criterion in compression.

3.2.1 Tension: A Rankine-Type Criterion

An adequate formulation of the Rankine criterion reads as a single function governed by the first principal stress and one yield value $\bar{\sigma}_t$ that rules the hardening/softening of the material:

$$f_1 = \frac{\sigma_x + \sigma_y}{2} + \sqrt{\left(\frac{\sigma_x - \sigma_y}{2}\right)^2 + \tau_{xy}^2} - \bar{\sigma}_t(\kappa_t) \tag{5}$$

where κ_t is the scalar that governs the amount of hardening/softening. Considering the three symmetric planes xy, yz, and xz, designated as $i = 1$, 2, and 3, respectively, one can write Eq. (5) in a matrix form:

$$f_i = \left(1/2\, \boldsymbol{\xi}_i^T \boldsymbol{P}_{t,i} \boldsymbol{\xi}_i\right)^{1/2} + 1/2\, \boldsymbol{\pi}_i^T \boldsymbol{\xi}_i \tag{6}$$

Here, $\boldsymbol{\xi}_i$ is the reduced stress vector given by $\boldsymbol{\xi}_i = \boldsymbol{\sigma} - \boldsymbol{\eta}_i$. The stress vector $\boldsymbol{\sigma}$ represents the six-components of the stress field and reads as $\boldsymbol{\sigma} = \{\sigma_x, \sigma_y, \sigma_z, \tau_{xy}, \tau_{yz}, \tau_{xz}\}^T$; the back stress vector $\boldsymbol{\eta}_i$ is given as $\boldsymbol{\eta}_1 = \{\bar{\sigma}_{tx}(\kappa_{t,1}),\ \bar{\sigma}_{ty}(\kappa_{t,1}), 0, 0, 0, 0\}^T$ for the xy-plane, as $\boldsymbol{\eta}_2 = \{0, \bar{\sigma}_{ty}(\kappa_{t,2}), \bar{\sigma}_{tz}(\kappa_{t,2}), 0, 0, 0\}^T$ for the yz-plane, and $\boldsymbol{\eta}_3 = \{\bar{\sigma}_{tx}(\kappa_{t,3}), 0, \bar{\sigma}_{tz}(\kappa_{t,3}), 0, 0, 0\}^T$ for the xz-plane. Likewise, the projection vector reads $\boldsymbol{\pi}_1 = \{1, 1, 0, 0, 0, 0\}^T$, $\boldsymbol{\pi}_2 = \{0, 1, 1, 0, 0, 0\}^T$, and $\boldsymbol{\pi}_3 = \{1, 0, 1, 0, 0, 0\}^T$. The projection matrix $\boldsymbol{P}_{t,i}$ is defined for each of the indexes 1, 2, 3 as:

$$\boldsymbol{P}_{t,1} = \begin{bmatrix} 1/2 & -1/2 & 0 & 0 & 0 & 0 \\ 0 & 1/2 & 0 & 0 & 0 & 0 \\ & & 0 & 0 & 0 & 0 \\ & & & 2\alpha_1 & 0 & 0 \\ & \text{sym} & & & 0 & 0 \\ & & & & & 0 \end{bmatrix} \quad \boldsymbol{P}_{t,2} = \begin{bmatrix} 0 & 0 & 0 & 0 & 0 & 0 \\ 0 & 1/2 & -1/2 & 0 & 0 & 0 \\ & & 1/2 & 0 & 0 & 0 \\ & & & 0 & 0 & 0 \\ & \text{sym} & & & 2\alpha_2 & 0 \\ & & & & & 0 \end{bmatrix}$$

$$\boldsymbol{P}_{t,3} = \begin{bmatrix} 1/2 & 0 & -1/2 & 0 & 0 & 0 \\ & 0 & 0 & 0 & 0 & 0 \\ & & 1/2 & 0 & 0 & 0 \\ & & & 0 & 0 & 0 \\ & \text{sym} & & & 0 & 0 \\ & & & & & 2\alpha_3 \end{bmatrix} \tag{7}$$

It is important to recall that the yield stress values $\bar{\sigma}_{tx}(\kappa_{t,i})$, $\bar{\sigma}_{ty}(\kappa_{t,i})$, $\bar{\sigma}_{tz}(\kappa_{t,i})$ are described by exponential softening rules:

$$\begin{aligned} \bar{\sigma}_{tx}(\kappa_{t,i}) &= f_{tx} \exp\left(-\frac{h f_{tx}}{G_{ftx}} \kappa_{t,i}\right) \\ \bar{\sigma}_{ty}(\kappa_{t,i}) &= f_{ty} \exp\left(-\frac{h f_{ty}}{G_{fty}} \kappa_{t,i}\right) \\ \bar{\sigma}_{tz}(\kappa_{t,i}) &= f_{tz} \exp\left(-\frac{h f_{tz}}{G_{ftz}} \kappa_{t,i}\right) \end{aligned} \tag{8}$$

where f_{tx}, f_{ty}, f_{tz} are the material uniaxial tensile strength values and G_{ftx}, G_{fty}, G_{ftz} the material tensile fracture energies according to the material axes; and h is the equivalent length related to the finite element size (Bažant and Oh, 1983), aiming the fracture energy regularization. A nonassociated plastic potential g_i has been considered and reads as:

$$g_i = \left(1/2\, \boldsymbol{\xi}_i^T \boldsymbol{P}_{g,i} \boldsymbol{\xi}_i\right)^{1/2} + 1/2\, \boldsymbol{\pi}_i^T \boldsymbol{\xi}_i \tag{9}$$

where $\boldsymbol{P}_{g,i}$ is the projection matrix that represents the Rankine plastic flow, given by Eq. (7) for an α_1, α_2, $\alpha_3 = 1$. The inelastic behavior is ruled by a strain-softening hypothesis, in which the scalar in rate form $\dot{\kappa}_{t,i}$ is written in terms of the plastic multiplier rate $\dot{\lambda}_{t,i}$, i.e., $\dot{\kappa}_{t,i} = \dot{\lambda}_{t,i}$.

3.3 Compression: A Hill-Type Criterion

A Hill-type criterion is used to characterize the yield condition of masonry in compression assuming a rotated centered ellipsoid shape. The formulation is considered in the 3D stress space for convenience and includes different compressive strength values along the different material axes. In a matrix form, the yield criterion can be written as:

$$f_4 = \left(1/2\, \boldsymbol{\sigma}^T \boldsymbol{P}_c \boldsymbol{\sigma}\right)^{1/3} - \bar{\boldsymbol{\sigma}}_c(\kappa_c) \tag{10}$$

where $\bar{\boldsymbol{\sigma}}_c$ is the yield value along the three material axes given by $\bar{\boldsymbol{\sigma}}_c(\kappa_c) = \sqrt[3]{\bar{\sigma}_{cx}(\kappa_c)\bar{\sigma}_{cy}(\kappa_c)\bar{\sigma}_{cz}(\kappa_c)}$. The projection matrix $\boldsymbol{P}_c$ is computed through Eq. (11):

$$\boldsymbol{P}_c = \begin{bmatrix} 2\frac{\bar{\sigma}_{cy}\bar{\sigma}_{cz}}{\bar{\sigma}_{cx}^2} & \beta_1 & \beta_2 & 0 & 0 & 0 \\ & 2\frac{\bar{\sigma}_{cz}\bar{\sigma}_{cz}}{\bar{\sigma}_{cy}^2} & 0 & 0 & 0 & 0 \\ & & 2\frac{\bar{\sigma}_{cx}\bar{\sigma}_{cy}}{\bar{\sigma}_{cz}^2} & 0 & 0 & 0 \\ & & & 2\gamma_1 & 0 & 0 \\ & \text{sym} & & & 2\gamma_2 & 0 \\ & & & & & 2\gamma_3 \end{bmatrix} \tag{11}$$

The parameters β_1, β_2 and γ_1, γ_2, γ_3 influence the shape of the yield criterion. The parameters β_i controls the coupling between the normal stress values and should be obtained experimentally (Lourenço, 1997), and the parameters γ_i are obtained as $\gamma_1 = (f_{cx}f_{cy})/\tau_{u,c}^2$, $\gamma_2 = (f_{cy}f_{cz})/\tau_{u,c}^2$, and $\gamma_3 = (f_{cx}f_{cz})/\tau_{u,c}^2$. Here, f_{cx}, f_{cy}, f_{cz} are the uniaxial compressive strengths in the x-, y-, and z-directions, respectively and $\tau_{u,c}$ the fictitious material pure shear strength in compression. The inelastic law of the material in the compressive regime comprehend a parabolic hardening followed by a parabolic/exponential softening, whereas different fracture energy values may be defined according to the material axes, i.e., G_{fcx}, G_{fcy}, and G_{fcz}.

The anisotropic macro-model has been implemented in the advanced software DIANA (2017) (strain-rate independent) and in ABAQUS (2013). In the latter, a FORTRAN user-subroutine VUMAT was developed, in which the material model and the procedure to update the stress vector and state variables has been provided.

3.4 A Simplified Multi-Scale (FE^2) Homogenization-Based Model

A simplified two-step numerical procedure has been recently introduced by the authors (Silva et al., 2017a,b). The aim has been the prediction of the static and dynamic mechanical response of periodic masonry structures, whereas both the masonry orthotropy and material nonlinear behavior can be represented under an attractive computational burden. The strategy makes use of a classical first-order homogenization scheme and is formed by three steps: (i) definition and solution of the meso-scale problem; (ii) implementation of the meso-to-macro transition; and (iii) solution of the macro-scale problem.

3.4.1 Meso-Scale (FE-Based Mesoscopic Model)

A unit-cell homogenization approach is employed at a meso-scale. The strategy can be designated as an upward procedure (i.e., information regarding the mechanical characterization at a cell level is transferred into the macro-scale). Different numerical models can be employed at a meso-scale and, therefore, the accuracy of the strategy is highly dependent on the accuracy of the latter. It relies on a micro-modeling approach and involves solving a mechanical problem on a representative volume element (RVE) to derive average field variables. The authors have employed a Kirchhoff–Love (KP) and a Mindlin–Reissner (MP) plate FE models but it is possible to use a three-dimensional model (3D DNS); see Silva et al. (2018) for further details. The units are elastic and the material nonlinearity is assumed to be lumped in the joints aiming at the decrease of the computational effort. This assumption seems to be specially adequate for strong block masonry structures (Sinha, 1978; Herbert et al., 2014). Units are modeled as quadrilateral FEs and mortar joints through zero-thickness interface FEs. The multi-surface plasticity model presented in Section 3.1 has been considered for the interface elements.

The RVE needs to be statistically representative of the macro-scale level (Hill, 1965) and sufficiently small to respect the principle of scales separation of first-order homogenization theory. Since a bespoken model for periodic masonries has been proposed (Silva et al., 2018), the recommendations by Anthoine (1995) are followed for the definition of the RVE within a running-bond and English-bond masonries. Accordingly, a rectangular pattern with more than one brick unit and within a rectangular basic cell is defined to represent the RVE of study, as seen in the next section. The RVE is herein denoted as Ω_m. The kinematical description of the homogenization-based models for

the in-plane case relies on the assumption that the macroscopic strain tensor $\boldsymbol{E}$ is obtained as the volume average of the mesoscopic strain field $\boldsymbol{\varepsilon_m} = \varepsilon_m(y)$ at each point over the associated RVE:

$$\boldsymbol{E} = \frac{1}{V_m} \int_{\Omega_m} \boldsymbol{\varepsilon_m} \, dV \tag{12}$$

where V_m is the volume of the RVE. The mesoscopic strain field can be decomposed into a macro-scale and meso-scale contribution. The latter is referred to as an additive decomposition of the mesoscopic strain tensor $\delta\boldsymbol{\varepsilon_m} = \delta\boldsymbol{\varepsilon_m}(y)$, and given as $\delta\boldsymbol{\varepsilon_m} = \delta\boldsymbol{E} + \nabla^s u_m$, where $\delta\boldsymbol{E}$ is the applied constant strain tensor over the RVE and $\nabla^s u_m$ is the gradient of the fluctuation displacement field. Considering that $\boldsymbol{\sigma_m}$ is the mesoscopic stress field, upon RVE equilibrium, the homogenized generalized stresses can be derived. The Hill–Mandell principle is based on an energetic equivalence between the macroscopic and mesoscopic work, as follows:

$$\boldsymbol{\Sigma} : \delta\boldsymbol{E} = \frac{1}{V_m} \int_{\Omega_m} \boldsymbol{\sigma_m} : \delta\boldsymbol{\varepsilon_m} \, d\Omega \tag{13}$$

in which $\boldsymbol{\Sigma}$ is the macroscopic stress tensor. According to the assumed additive decomposition of the mesoscopic strain tensor, one may obtain the macro-homogeneity principle as:

$$\boldsymbol{\Sigma} : \delta\boldsymbol{E} = \frac{1}{V_m} \int_{\Omega_m} \boldsymbol{\sigma_m} : \delta\boldsymbol{E} \, d\Omega + \frac{1}{V_m} \int_{\Omega_m} \boldsymbol{\sigma_m} : \nabla^s \delta u_m \, d\Omega \tag{14}$$

for any kinematical admissible δu_m. Periodic boundary conditions are assumed to solve the boundary value problem. Such consideration is extensively found in homogenization procedures (Blanco et al., 2016) also for the particular case of masonry structures (Cecchi and Sab, 2002b; Milan et al., 2006a; Otero et al., 2015). The periodic boundary conditions lead to a kinematical field that enforces anti-periodicity of the tractions to occur. Due to the periodicity of the displacement fluctuations on the boundaries, Eq. (14) can be simplified and expressed as:

$$\boldsymbol{\Sigma} : \delta\boldsymbol{E} = \frac{1}{V_m} \int_{\Omega_m} \boldsymbol{\sigma_m} : \delta\boldsymbol{E} \, d\Omega, \; \forall \, \delta\varepsilon \tag{15}$$

Thus, the corollary of the Hill–Mandell principle is that the homogeneous macroscopic stress tensor $\boldsymbol{\Sigma}$ can be written as the volume average of the mesoscopic stress field $\boldsymbol{\sigma_m} = \boldsymbol{\sigma_m}(y)$ over the RVE:

$$\boldsymbol{\Sigma} = \frac{1}{V_m} \int_{\Omega_m} \boldsymbol{\sigma_m} \, d\Omega \tag{16}$$

The variational principle and the use of periodic boundary conditions allow concluding that the external surface tractions and body force field on the RVE are reactive terms over the imposed kinematical conditions. These kinematical boundary conditions are dependent on the deformation modes considered at the meso-mechanical level. Thus, the in-plane static equilibrium of the RVE is reached for each kinematic constraint considered, without any external surface traction and body force terms. The variational principle holds when accounting for the out-of-plane quantities to assure the energy consistency between scales. The difference lies in the replacement of generalized stresses through moment and force terms.

The homogenization technique is followed and, by solving the internal static RVE equilibrium using a classical FE-procedure, the homogenized $\boldsymbol{\Sigma}$ and $\boldsymbol{E}$ quantities are derived. Furthermore, the macro-stress couples are obtained by through-the-thickness integration of the homogeneous macro-stresses according to Eq. (17); wherein i, j refers to the index x or y (M_{xx}, M_{xy}, M_{yy}). The numerical integration is performed accounting only the mid-plane reference surface ω. The obtained homogenized moment-curvature relations are defined per unit of length.

$$M_{ij} = \int_{-z/2}^{z/2} \boldsymbol{\sigma}_{m,ij} z \, dz \tag{17}$$

3.4.2 Macro-Scale (FE Discrete Model)

Discrete FE-method based strategies, designated in the literature as rigid body spring models (RBSMs), represent masonry as the assembly of rigid blocks interconnected by discrete interfaces whereas the deformation is represented through normal and tangential springs. RBSMs are supported in the theoretical background of Kawai (1978) works. Yet some differences exist between RBSMs and other discrete-based strategies, as the discrete (or distinct) element method (DEM) or the applied element method (AEM). In fact, FE methods may not be so efficient for problems in which several physical discontinuities exist in the media leading to a situation where several distinct bodies exhibit large relative movements. In such problems, where the contact conditions vary during the analysis and large displacements are expected, using the DEM strategy for the masonry modeling seems the best choice (Cundall and Hart, 1971; Lemos, 2007). DEM is, however, based on explicit numerical procedures and its usage within a dynamic analysis of masonry structures can be prohibitive due to the involved computational processing times. Concerning the AEM, first proposed by Meguro and Tagel-Din (2000), it has features analogous to the RBSMs. It represents masonry through the assembly of rigid elements interconnected by discrete interfaces that are also modeled through normal and shear nonlinear springs. The main differences between AEM and RBSM are that the former assumes recontact between neighboring discrete elements after the occurrence of collapse and that it tends to employ a micro-modeling approach to describe masonry (Guragain et al., 2006; Malomo et al., 2018). The latter can be a contentious issue when engineering larger structures. In converse, RBSMs allow to adopt coarser scales meshes within a macro-modeling approach for masonry and, therefore, increase the computational efficiency.

Several RBSMs are mentioned in the literature, as the one implemented by Caliò et al. (2012) for the in-plane study of masonry and extended to the out-of-plane application by Pantò et al. (2017) and Casolo (1999) who investigated the out-of-plane behavior of a masonry façade. The latter RBSM strategies are quite promising from a computational standpoint but demand the calibration of both the material and mechanical properties assigned to the nonlinear springs. Such a procedure can lead to loss of the physical meaning of the input parameters and may be arguable in cases where experimental evidence is lacking. Hence some authors coupled different RBSMs within two-scale strategies, wherein the material information of the springs is computed through homogenization strategies. For instance, Milani et al. (2006) implemented a limit analysis-based two-scale strategy in which an RBSM, represented through rigid triangular constant stress elements and rotational interface springs, is linked with a simple homogenization strategy for the study of URM panels. Similarly, Casolo and Milani (2010) and Casolo and Uva (2013) adopted, respectively, a homogenization-based RBSM using quadrilateral rigid elements and rotational interface springs for the nonlinear static and dynamic analysis of masonry structures, respectively. The existing strategies typically focus on the out-of-plane behavior only and in the use of simplified analysis methods at a macro-scale, as limit-analysis, to improve the strategies robustness in the presence of material softening for quasi-static problems.

In such a context, a discrete FE-method based procedure is proposed and implemented into the advanced finite element software ABAQUS (2013). It stems from the RBSM model presented by Silva et al. (2017a,b), which is suitable only for the out-of-plane analysis of masonry structures. Thus, an improved and innovative RBSM is here addressed as it incorporates both the in- and out-of-plane behavior of masonry being also coupled with the presented novel homogenization strategy.

The RBSM model is composed by the assemblage of discrete quadrilateral rigid plate elements interconnected, at its interfaces, through a set of rigid and deformable truss FEs; see Fig. 3 (equivalent to spring elements). The truss elements govern both the deformation and damage of the structure by being able to mimic the presence of the in- and out-of-plane failure modes considered in Fig. 3 and within a decoupled characterization. These can append the material information of the meso-scale homogenized step and thus represent the masonry texture via an equivalent continuum medium.

The two-scale simplified procedure allows processing the meso- to macro-scale transition only once and, therefore, achieve low computational times. The main advantages of the procedure are threefold: (1) several strategies with different complexities can be employed at a meso-scale; (2) the concrete damage plasticity (CDP) model implemented in ABAQUS can properly characterize the constitutive material model of the truss elements at a macro-scale, as it suitable to fully reproduce the homogenized response of the masonry RVE; and (3) the computational robustness

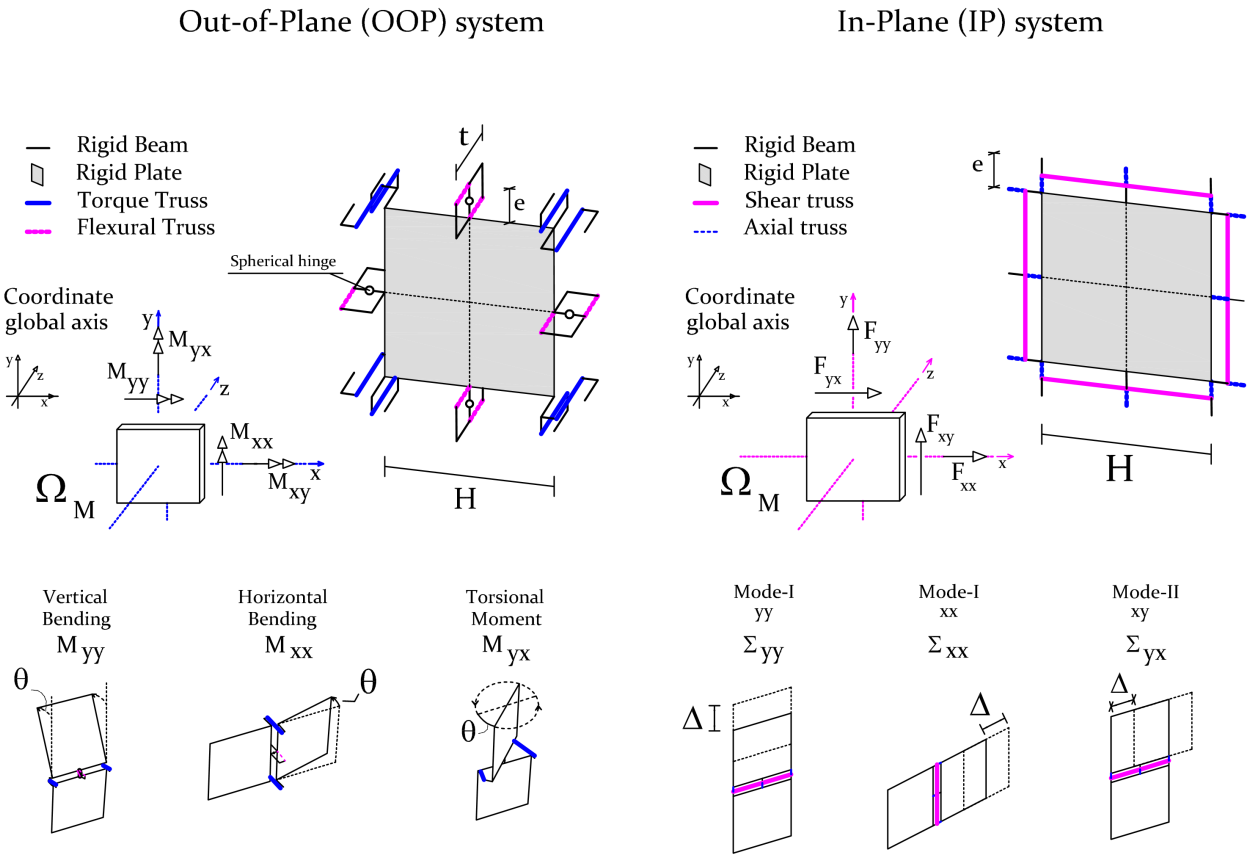

FIG. 3: Description of the basic in- and out-of-plane FE truss/beam systems of the discrete macro-unit cell

in presence of material softening can be guaranteed for quasi-static problems by arc-length procedures available in ABAQUS software.

Specifically, the model combines a stress-based plasticity with a strain-based scalar damage and can reproduce several macroscopic properties for tension and compression regimes, such as different yield strengths which represent masonry orthotropy; different stiffness degradation values which represent the masonry full softening behavior; different recovery effect terms; and rate sensitivity, which can increase the peak strength value depending on the response strain rate. Moreover, it does consider the latter in the presence of interfaces dynamic and/or cyclic loading and is integrated using the backward Euler method. A general overview of the main features of CDP for the rate-independent model are presented next; see Lubliner et al. (1989) and Lee and Fenves (1998) for further details.

Effective stresses govern the plastic part of these models (Grassl and Jirásek, 2006) and the stress-strain relationship is ruled, as referred, by an isotropic damage scalar affecting the elastic stiffness of the material. The nominal stress tensor $\boldsymbol{\sigma}$ reads:

$$\boldsymbol{\sigma} = (1-d)\boldsymbol{E}_0^{el} : \left(\boldsymbol{\varepsilon} - \boldsymbol{\varepsilon}^{pl}\right) = \boldsymbol{E} : \left(\boldsymbol{\varepsilon} - \boldsymbol{\varepsilon}^{pl}\right) \tag{18}$$

where $\boldsymbol{E}_0^{el}$ is the initial elastic stiffness of the material; d is the damage parameter, which defines the stiffness degradation (0 for an undamaged and 1 for a fully damaged material), and is designated as d_t and d_c for tension and compression regimes, respectively; $\boldsymbol{\varepsilon}$ is the total strain tensor; $\boldsymbol{\varepsilon}^{pl}$ is the plastic strain tensor, and $\boldsymbol{E}$ is the initial elastic stiffness of the material affected by the damage parameters [the degraded initial stiffness given by $\boldsymbol{E} = (1-d)\boldsymbol{E}_0^{el}$].

A nonassociated flow-rule is assumed for the plasticity model and given by:

$$\dot{\boldsymbol{\varepsilon}}^{pl} = \dot{\lambda}\frac{\partial g_p}{\partial \bar{\boldsymbol{\sigma}}}\left(\bar{\boldsymbol{\sigma}}, \boldsymbol{\kappa}_p\right) \tag{19}$$

in which $\dot{\boldsymbol{\varepsilon}}^{pl}$ is the rate of the plastic strain, $\dot{\lambda}$ is the rate of the plastic multiplier, g_p is the plastic potential, $\bar{\boldsymbol{\sigma}}$ is the effective stress tensor, and $\dot{\boldsymbol{\kappa}}_p$ is the hardening/softening variable. The rate of the hardening/softening variable $\dot{\boldsymbol{\kappa}}_p$ is related to the rate of plastic strain given by an evolution law $\boldsymbol{h}$, as seen in Eq. (20):

$$\dot{\boldsymbol{\kappa}}_p = \boldsymbol{h}\left(\bar{\boldsymbol{\sigma}}, \boldsymbol{\kappa}_p\right) : \dot{\boldsymbol{\varepsilon}}^{pl} \tag{20}$$

The CDP model uses a yield function based on the works of Lubliner et al. (1989) and Lee and Fenves (1998). The hardening parameter that controls the meridians shape of the yield shape is given by $K_c = 2/3$, which leads to an approximation of the Mohr–Coulomb criterion.

Hence, following the input requirements for the CDP model, it is mandatory to obtain effective stress and strain curves for each angle of the interface and for each bending moment direction. In other words, the material orthotropy is reproduced at a structural level because the approach offers the possibility to reproduce different input stress-strain relationships according to the trusses plane. To what concerns the in-plane behavior, the stress quantities are directly derived from the mesoscopic homogenized values scaled according to the length of the macro-interfaces. For the out-of-plane behavior, the conversion from moment to stress values must be achieved following Eqs. (21) and (22):

$$\sigma_{\text{Bending truss}} = \frac{M}{A_{\text{Bending truss}} \times e} \tag{21}$$

$$\sigma_{\text{Torsional truss}} = \frac{M}{A_{\text{Torsional truss}} \times H} \tag{22}$$

Here, M is the bending moment per unit of interface length, H the length of each quadrilateral panel (L is the influence length of each truss and is equal to half of the mesh size, i.e., $H/2$), t is the thickness of the wall, $A_{\text{Bending truss}}$ and $A_{\text{Torsional truss}}$ are the bending and torsional truss areas, respectively, and are given by $0.5 \times e \times H$ where e (value of 10 mm) is the gap between the rigid plates, which ideally should be zero but in practice is assumed small enough to be able to place trusses between elements.

At last, the stress homogenized input curves may be properly calibrated (so-called regularization). An elastic calibration for the stress curves is conducted. The latter is guaranteed separately for both in-plane and out-of-plane modes and, therefore, a decoupled behavior is derived. Briefly, by assuring the energy equivalence between the discrete mechanism and a homogeneous continuous plate element, it can be easily derived that, for both case studies, the Young's moduli of axial, shear, bending, and torsional truss elements is given as:

$$E_{ii}^{\text{in-plane axial truss}} = \frac{\bar{E}_{ii}e}{4L + 2e}; \quad E_{xy}^{\text{in-plane shear truss}} = \frac{\bar{G}_{xy}H^2}{4e(2L + e)} \tag{23}$$

$$E_{ii}^{\text{Bending truss}} = \frac{\bar{E}_{ii}t^4H}{12(1 - \nu^2)(H + e)e^3H}; \quad E^{\text{Torsional truss}} = \frac{2\bar{G}_{xy}t^4}{3H^2e(2L + e)} \tag{24}$$

where $\bar{G}_{xy}$ is the homogenized shear modulus given directly by the slope of the shear meso-scale homogenized curve; $\bar{E}_{ii}$ is the Young's moduli of the masonry in the direction ii (i represents the cartesian axis x or y); and ν is the Poisson coefficient for the homogeneous media. After the calibration and aiming to fulfill the input requirements for the CDP model in ABAQUS, the information regarding the post-failure behavior may be introduced for each element that features material nonlinearity in terms of effective stress and inelastic strain $\tilde{\varepsilon}^{ck}$ values (i.e., the truss elements). Since truss elements define the material behavior of the macro-interfaces, the system will undergo only uniaxial loading conditions. Hence, for the case of uniaxial loading condition, the inelastic strain value must be obtained for each point of the post-peak homogenized curve according to Eq. (25):

$$\tilde{\varepsilon}^{ck} = \varepsilon - \varepsilon_0^{el} \tag{25}$$

where ε_0^{el} is the elastic strain corresponding to the undamaged material and ε is the total axial strain of the multi-linear stress envelope. If the damage parameter d are introduced, the plasticity model is thus coupled with a damage description and is suitable for the cyclic behavior description of the material. Again, for the case of uniaxial loading condition and for a given truss element, the plastic strain values ε^{pl} are calculated for each point of the input curve through Eq. (26). Since the permanent plastic strains values ε^{pl} can be just positive or null, the latter can constitute a good checkpoint to foresee if the damage parameters have been properly computed.

$$\varepsilon^{pl} = \varepsilon^{cr} - \frac{d}{1-d}\frac{\sigma^P}{E_0^{el}} \tag{26}$$

In continuum FE-based frameworks, in which material nonlinearity and cracking are attributed to continuum elements [through, for instance, the proposed anisotropic macro-model or other models, as the smeared crack by Rots et al. (1985)], the strain localization is a key issue and the regularization of the FE material constitutive law is necessary to achieve mesh objectivity of the results. In related multi-scale continuum, FE approaches (see Cervera and Chiumenti, 2006; Petracca et al., 2016) an alike procedure is implemented. This is typically based on the crack band theory by Bažant and Oh (1983), whereas the definition of a characteristic length that addresses both scales is required to affect the fracture energy of the material constitutive model.

For the present homogenization-based strategy, the mesh objectivity problem resorts only on the correction of the material homogenized data according to the discrete macro-mesh refinement rather than the strain localization issue at both scales. This is so because, at a meso-scale, both the material nonlinearity and cracking are placed on mortar joints that are modeled in a discontinuous (interface elements) way (Borst et al., 2006); and, at a macro-scale, an RBSM is adopted in which material softening and cracking is lumped on individual 2-node linear truss elements (one integration point), for which a characteristic length of 1 is generally given (ABAQUS, 2013; DIANA, 2017).

Thus, the so-called regularization step is here performed aiming to correct the elastic stiffness and post-peak fracture energies of the stress-strain curves that serve as input for the CDP model. The derived meso-scale homogenized curves (per interface unit length) are first scaled, according to the macro-interface length H, and second affected by a regularization factor f_r depending on if it represents an in-plane (normal and shear) or an out-of-plane (flexural and torsional) mode.

Consider, for instance, that $\tilde{E} = [\varepsilon_1 \ \varepsilon_2 \ \cdots \ \varepsilon_{n-1} \ \varepsilon_n]$ and $\tilde{\Sigma} = [\sigma_1 \ \sigma_2 \ \cdots \ \sigma_{n-1} \ \sigma_n]$ are the n-dimensional vectors which define, respectively, the σ-ε homogenized curve being regularized (n is the number of points of the curve). After scaling the stress values of $\tilde{\Sigma}$ according to the macro-scale mesh size, it is required to regularize the strain values of $\tilde{E}$. In this regard, the regularization factor f_r, is, for a given truss element set, defined as the relation between the elastic stiffness of the σ-ε curve under study and the calibrated Young modulus obtained for each deformable truss through Eqs. (23)–(24). The procedure to compute the reference elastic stiffness value is assumed to be performed for the designated point C; the point of the σ-ε homogenized curve that has a stress given as one-third of the peak value. Thus, f_r is computed as $f_r = \sigma_C/(\varepsilon_C E_{\text{calibrated}})$ where, $E_{\text{calibrated}}$ is the corrected Young modulus obtained for each truss type following Eqs. (23)–(24).

In other words, the regularization terms can be simply written as $f_r^{\text{mode-I}} = \bar{E}_{ii,C}/E_{ii}^{\text{in-plane axial truss}}$ and $f_r^{\text{mode-II}} = \bar{G}_{xy,C}/E_{xy}^{\text{in-plane shear truss}}$ for the in-plane macro-trusses; and as $f_r^{\text{bending}} = \bar{E}_{ii,C}/E_{ii}^{\text{bending truss}}$ or $f_r^{\text{torsion}} = \bar{E}_{xy,C}/E_{xy}^{\text{torsional truss}}$ for the out-of-plane macro-trusses. Such parameters f_r affects all the strains of the homogeneous stress-strain curves of the corresponding trusses. By correcting the strain axis to calibrate the elastic stiffness value the operator affects, as well, the post-peak curve strains and so, in an implicit way, the fracture energy itself. It may be pointed out that, for the out-of-plane truss elements (both the torsion and bending elements), the scaling and the regularization steps are performed only after the conversion of homogenized moment values into stress quantities according to Eqs. (21) and (22).

3.5 Strain-Rate Dependency of the Modeling Strategies

The use of static strength properties can lead to inaccurate results when evaluating the masonry behavior under fast dynamic actions since these properties exhibit an enhancement according to the strain rate level of the applied load.

Research mainly centered on concrete-like materials can be found in the literature, where assumptions intrinsically related with material effects are reported to explain the phenomena, such as the lateral inertial confinement, end support friction and scale-effect (Le Nard and Bailly, 2000; Hao et al., 2013; Hao and Hao, 2013).

Experimentation is, in the field of fast dynamics, still at a higher level with respect to numerical modeling (Buchan and Chen, 2007). Some laboratory tests have been performed to evaluate the response of the masonry under such extreme loads, see Dennis et al. (2002), Baylot et al. (2005), Hao and Tarasov (2008), Pereira et al. (2015), Pereira and Lourenço (2016a,b). In converse, few numerical studies on the response of masonry under blast or impact actions are found in the literature: Wu et al. (2005), Burnett et al. (2007), Zapata and Weggel (2008), Macorini and Izzuddin (2014).

The strain-rate dependency of the masonry can be represented through the use of visco-elastic models aiming at strain-rate regularization (Sluys and De Borst, 1992; Georgin and Reynouard, 2003). This seems an adequate and numerically convenient strategy, especially if one notices that introducing, for instance, the well-known Duvaut and Lions (1976) model within an FE plasticity model is well documented. Yet the definition of a viscosity regularization parameter still lacks objectivity and requires extensive sensitivity studies for the case of masonry.

In such a context, the presented inviscid advanced FE formulations have been formulated to account for this phenomenological feature of masonry by making use of dynamic increase factors (DIFs). The authors believe that these numerical models may strongly contribute to further advances on this complex topic. The DIFs directly affect the static material properties adopted and can be introduced in the strategies via: (i) a strain-rate law, typically a logarithmic curve, for each selected parameter; or (ii) a discrete DIF value, independent from the strain rate level, which is *a priori* assumed and adopted as constant. The former may yield more realistic values, but the latter is straightforward, simple and more aligned with normative proposals. These data can be deduced through experimental campaigns as seen in Pereira and Lourenço (2016a) and Hao and Tarasov (2008).

According to the information at disposal, different DIF values are obtained for each mechanical parameter of masonry, which allows the expansion or contraction of the strength envelope, thus depending on the load strain-rate; as schematically described in Fig. 4 for the case of the composite interface model.

4. APPLICATIONS

4.1 Engineering a Meso-Scale Mechanical Problem

The majority of the existing research on periodic masonry deal with running-bond texture within the case of a single-wythe wall (Zucchini and Lourenço, 2002; Milani, 2008; Pau and Trovalusci, 2012; Taliercio, 2014; Reccia et al., 2018). Some features still somehow seem under-investigated, as: (i) the analysis of the effect of potential

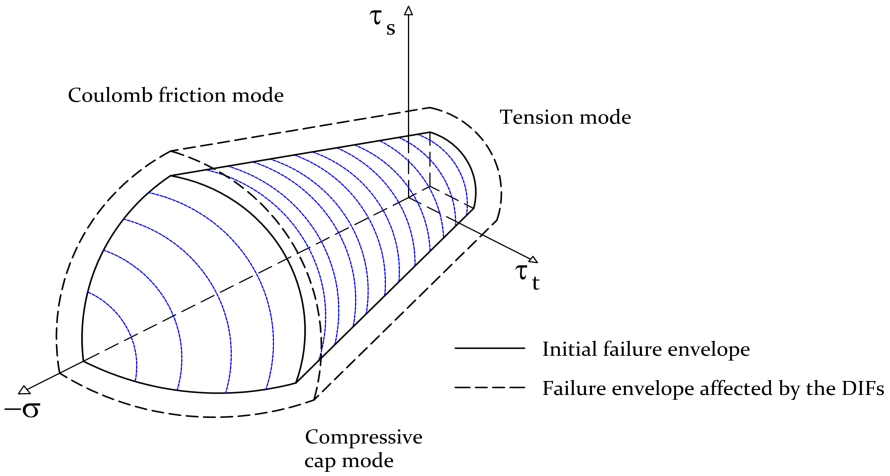

FIG. 4: Schematic representation of the yield envelope for the composite interface model adopted affected by the DIFs

discontinuities in the masonry thickness, when two- or three-wythes of masonry are present; (ii) the effect of three-dimensional shear stresses; and (iii) the study of other periodic textures, as the English-bond.

In this context, a study at a meso-scale is presented next. This is aimed to assess the mechanical effect of the mid-thickness vertical joint of English-bond masonry walls and the effect that three-dimensional shear stresses play. The conclusions are drawn in terms of moment-curvature curves.

The selected case study concerns the English-bond masonry tested experimentally by Candeias et al. (2017). The problem is schematically described in section Fig. 5(a), which accounts for three unit-cell models. The first-unit cell

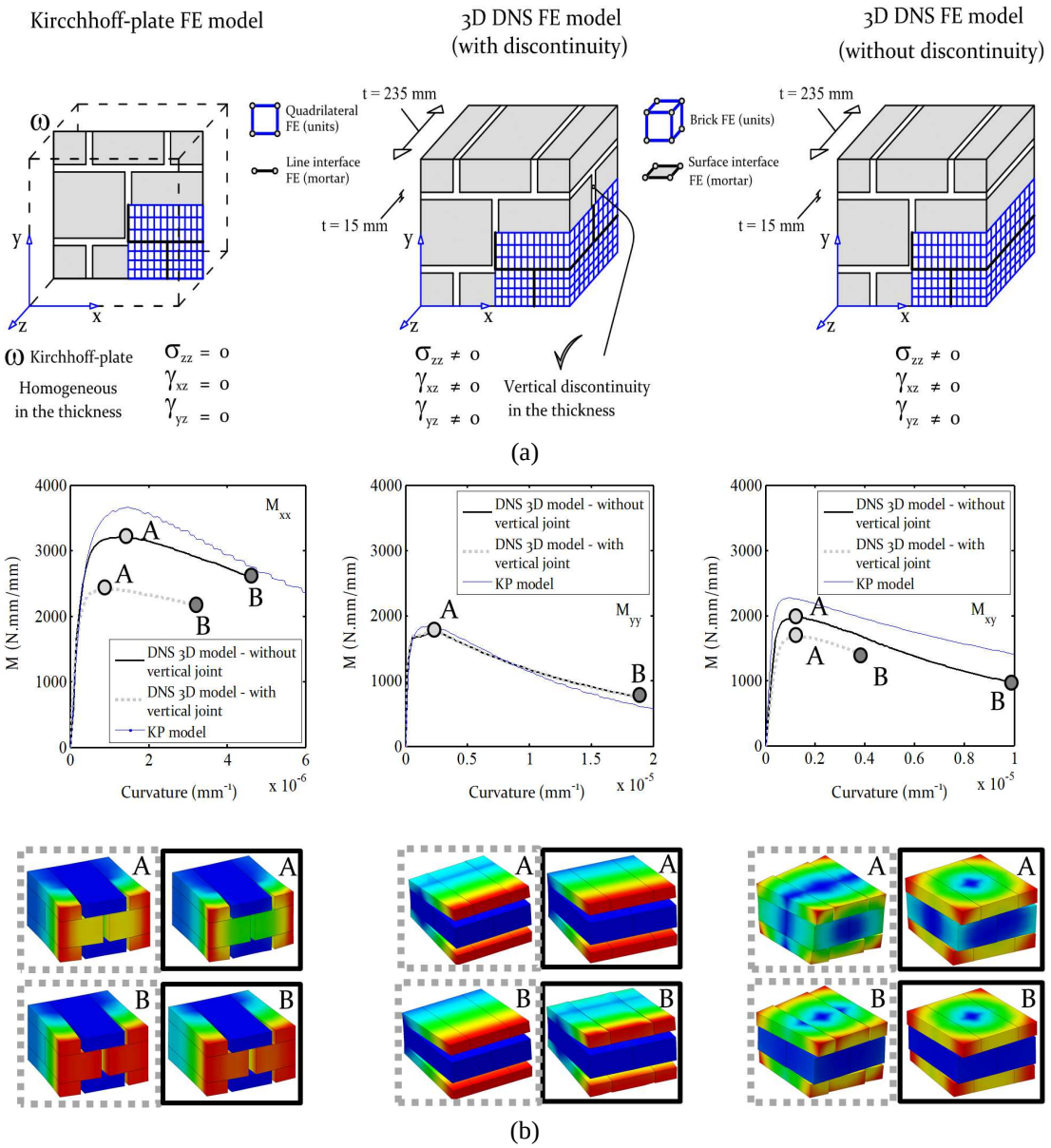

FIG. 5: Meso-scale mechanical study of an English-bond masonry texture: (a) numerical models assumed for the RVE description; (b) results obtained in terms of moment vs. curvature curves using a KP model and two DNS 3D models: one that considers, and the other that excludes the existent vertical joint on the mid-thickness. Deformed configurations at peak and ultimate post-peak point are plotted for both models.

model advents from a Kirchhoff-plate mesoscopic model in which the aforementioned homogenization scheme (see Section 3.3) is followed. The remaining two unit-cell models follow a direct numerical simulation (DNS models) or a micro-modeling approach (as referred in Section 3.1): the latter does not take into account the discontinuity along with the thickness, whereas the former considers it, meaning that it is explicitly modeled. The adopted material properties for units are $E_u = 11{,}000$ MPa; $v_u = 0.25$ and for mortar joints $E_m = 2{,}200$ MPa; $v_m = 0.20$; and the inelastic mechanical parameters for mortar joint interfaces are given by: $f_t = 0.105$ MPa, $G_f^I = 0.012$ N/mm, $c = 0.20$ MPa, $G_f^{II} = 0.05$ N/mm, $\phi = 30$ degrees, $f_c = 2.84$ MPa; $G_f^{IV} = 4.00$ N/mm. For all the cases, the material nonlinearity is lumped in the mortar joints by using interface FEs within the presented multi-surface plasticity model. Note that the linear elastic relation between the generalized stresses and strains of the interface FEs is given by the classical constitutive equation of Hooke's law, $\boldsymbol{\sigma} = \boldsymbol{D}\boldsymbol{\varepsilon}$. Considering a line FE interface [for the adopted plate theories Kirchhoff–Love (KP) and a Mindlin–Reissner (MP) models], the elastic stiffness matrix $\boldsymbol{D}$ is given as $\boldsymbol{D} = \mathrm{diag}\{k_n, k_s\}$. The values of the normal (k_n) and shear (k_s) mortar joints stiffness terms can be easily computed through Eqs. (27) and (28), if considered that the masonry components are represented by a serial chain of springs, under a stack-bond, with uniform stress distributions in both the unit and mortar joints. Therefore, the obtained values for $k_n = 183$ N/mm; $k_s = 72.6$ N/mm, respectively.

$$k_n = \frac{E_u E_m}{t_m(E_u - E_m)} \tag{27}$$

$$k_s = \frac{G_u G_m}{t_m(G_u - G_m)} \tag{28}$$

where $t_m = 15$ mm is the thickness of the mortar joints; G_u and G_m are the shear modulus of the unit and mortar, respectively. Figure 5(b) shows the obtained results. It is noted that the presence of the vertical discontinuity in the masonry thickness has a marginal effect on the RVE vertical bending behavior M_{yy}. On the contrary, the model with the discontinuity manifests a lower capacity for both the horizontal M_{xx} and torsional M_{xy} moments with differences ranging the 33% and 17%, respectively. Additionally, if the KP model results are considered, an error of 52% is expected for the horizontal bending moment case. Such results prove the importance of addressing the mortar discontinuities and the three-dimensional shear effects along the thickness of a masonry wall; especially in cases where the thickness value is significant, as seen in Silva et al. (2018). Also, this highlights the care that needs to be taken when adopting a modeling strategy for a given case study. The total processing time (CPU time requirements using a laptop with an i7-4710MQ CPU) of the simulations was 81 s, 246 s, and 249 s for the KP model, DNS model without discontinuity and DNS model with discontinuity, respectively.

4.2 Engineering Complex Problems: Meso/Macro Scales

4.2.1 LNEC Brick-House Mock-Up

The selected case study comes from the experimental work performed in LNEC by Candeias et al. (2017), which was developed to foster a blind test prediction by different invited authors on the dynamic behavior of a masonry structure. The studied brick structure is composed of three walls in a U-shaped plan arrangement. The main façade (East plan) presents a gable wall and is linked with two transversal walls that act as abutments (North and South plans). These were constructed with clay brickwork in an English-bond arrangement of 235 mm of thickness (slenderness ratio about 1:10). The geometrical features are seen in Fig. 6(a). The brick mock-up was tested until collapse in a shaking table under a unidirectional seismic loading. The seismic input was applied in a perpendicular direction (E-W) to the main façade and derives from the N64E strong ground motion component associated with the February 21, 2011 earthquake that occurred in Christchurch, New Zealand. After the filtering and cropping, the latter time signal served as a reference for the seismic input generation and is composed of eight accelerograms. These have been obtained from a scaling process, starting from one up to three. The input signal considered in the dynamic analysis is displayed in Fig. 6(b).

Two (out of three) of the presented numerical approaches are used for this analysis as depicted in Fig. 6(c). In particular, the macroscopic model and the simplified two-scale model. Again, the former represents masonry as an

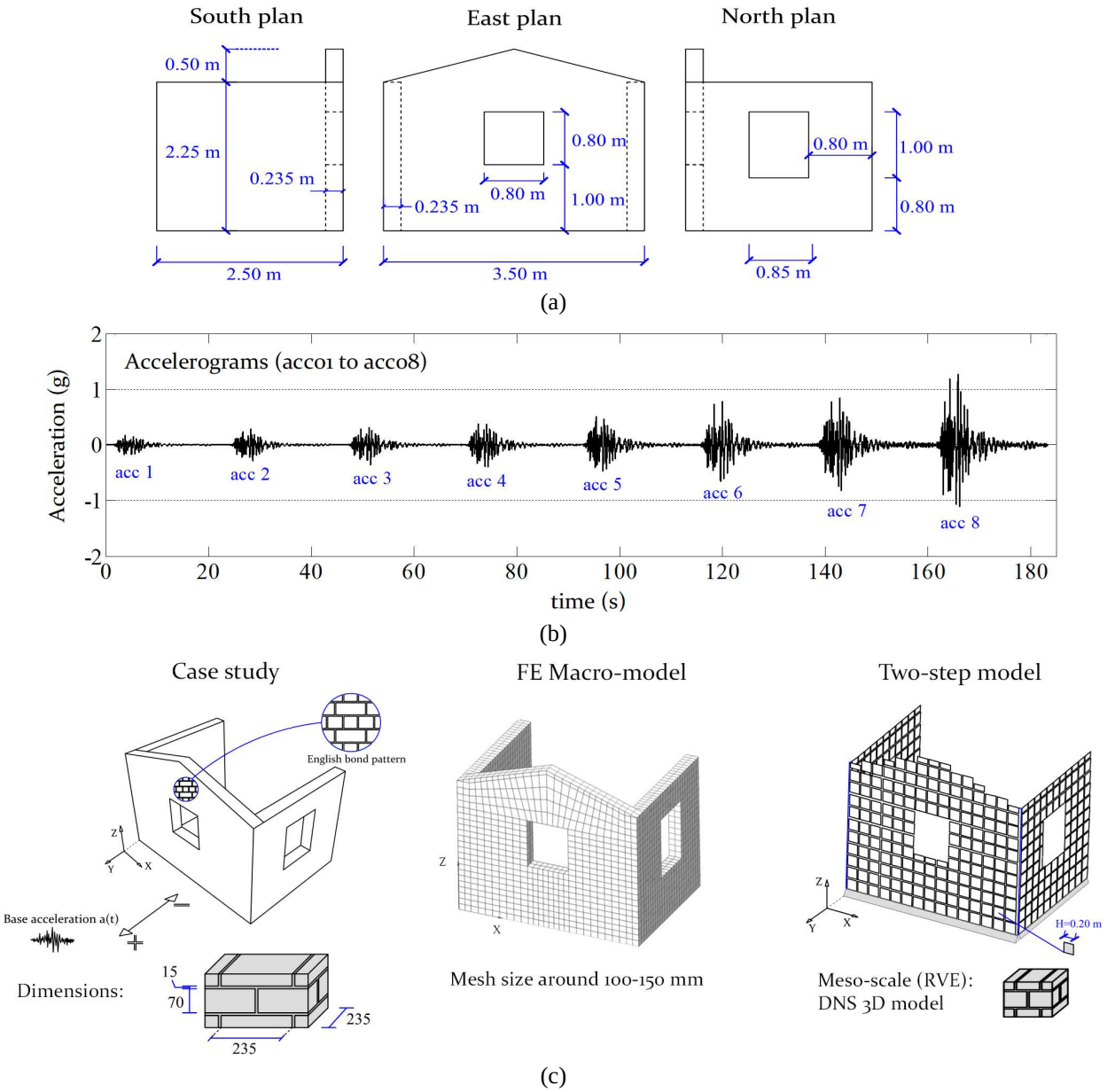

FIG. 6: Case study: (a) the geometry of the case study; (b) the experimental input seismic signal; (c) case study and the numerical models considered for the dynamic analysis

isotropic material and has been defined here to follow a total strain rotating crack constitutive material model, whereas an exponential and parabolic law is adopted, respectively, for the tensile and compressive behaviors. An approximated mesh size of 100 up to 150 mm was defined using 3D finite elements, and such fine discretization intends to by-pass numerical problems faced during the performed computations. For the latter, a direct numerical simulation (DNS 3D mode with discontinuity) has been assumed at a meso-scale to derive the homogenized quantities, wherein the vertical mortar discontinuity is present in the thickness direction. At a macro-scale, a mesh size of 200 mm is adopted.

The calibration of the elastic brickwork stiffnesses (E_{xx}, E_{xy}, and E_{yy}) has been reached by accounting with the modal identification data available. For the strength properties, as the tensile strength, cohesion, and compressive

strength, the values from Candeias et al. (2017) have been used. The parameters that control the material curves beyond the peak, namely the fracture energies, refer to typical masonry literature values and no experimental reference is known.

Dynamic analysis has been performed by subjecting the structure to the defined seismic input. Since the structure has collapsed for the last accelerogram (acc 8), the comparison is achieved for the accelerogram seven (acc 7) as shown in Fig. 7. The results give good indications of the ability of the presented two-step approach in the dynamic behavior prediction of the English-bond structure, as a good agreement was found with the experimental time-history displacements. Even if slight differences are visible for the peak displacements, the two-scale model also accurately reproduces the residual displacement.

On the other hand, the macroscopic model seems to overestimate the structure capacity. The response is far for being alike with the behavior reproduced by the latter procedure, despite sharing both the same material and mechanical input. The nonconsideration of the existent vertical discontinuity seems to be of utmost importance. In fact, the latter is paramount as it significantly decreases the bending and torsional capacities. Furthermore, the macroscopic approach makes use of a hysteretic behavior with secant unloading-reloading branches, a feature that leads to the underestimation of the energy absorption and is incapable to record permanent plastic deformations.

Additionally, Fig. 8 reports the observed experimental and numerical damage maps. From the two-scale and macroscopic models, a vertical crack in the gable wall (due to horizontal bending) is observed. In the former, the onset of cracking is registered as well, due to torsional movements in the east plan opening towards the corners. Both strategies captured moderate damage in the east-north corner, even if this is not clear from the experimental observations. Some in-plane damage around the north piers is also registered. In general, a reasonable agreement has been found for such a complex study. The total processing time (CPU time requirements using a laptop with an i7-4710MQ CPU) of the simulations was 76 min and 720 min for the two-scale (DNS 3D) model and the FE macro-model, respectively.

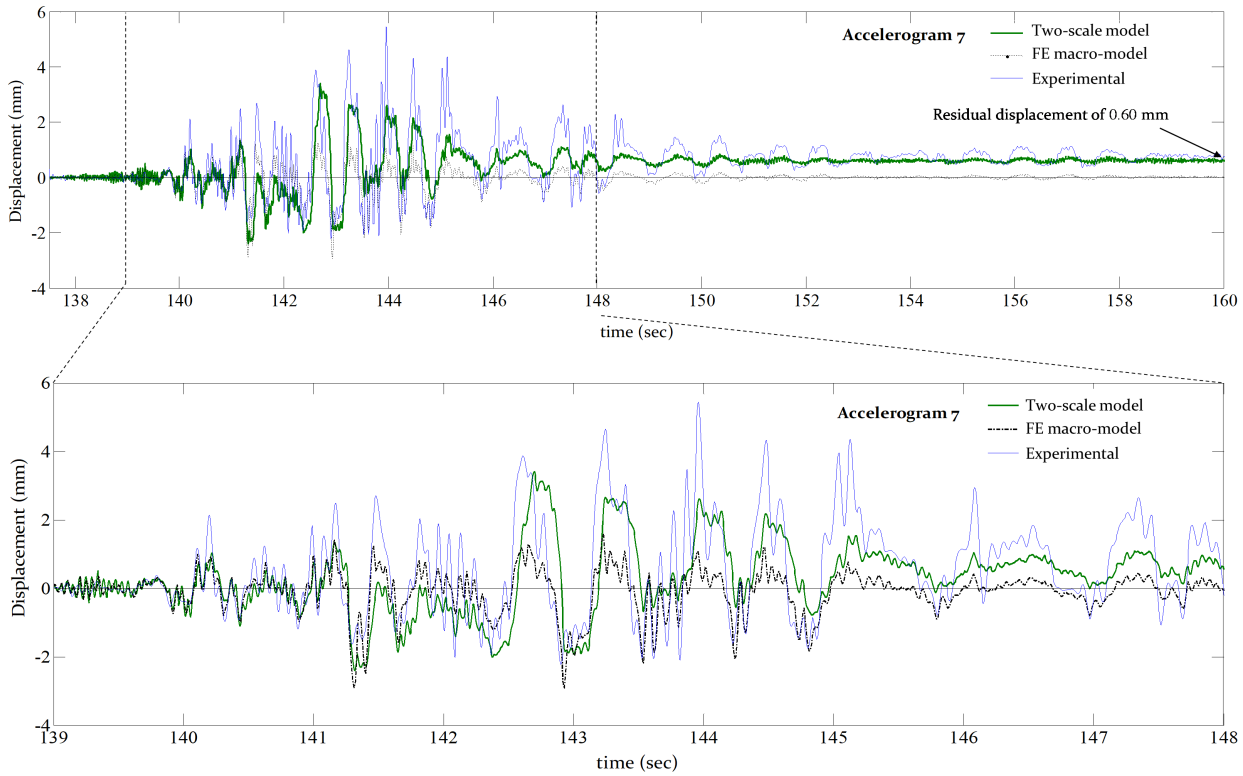

FIG. 7: The obtained time-history displacements for the last analyzed accelerogram (acc 7)

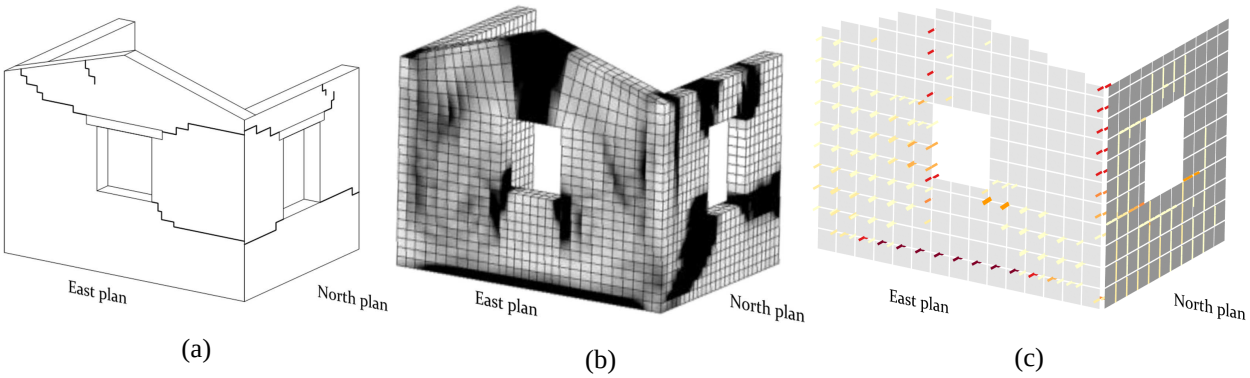

(a) (b) (c)

FIG. 8: Observed damage: (a) after the experimental series of seven accelerograms (from acc 1 to acc 7); (b) for the macroscopic model at the instant $t = 160$ s; (c) for the two-scale model at the instant $t = 160$ s

4.2.2 Sheffield University Parapet Wall

Experimental data available from the research reported by Gilbert et al. (2002a) was used to assess the ability of the presented numerical strategies in the prediction of the dynamic behavior of masonry when subjected to a low-velocity impact load. The numerical strategies presented in Section 3 are addressed [Fig. 9(a)–9(c)]. Note that a finer mesh refinement has been assumed for all the strategies.

The selected parapets are designated as C6 and C7 and are replicates. Their assemblage was executed with strong concrete blocks and weak mortar. The parapet walls and brick dimensions, as well as the boundary conditions assumed, are reported in Fig. 9(a). Aiming to model a vehicle-like impact at both mid-height and length of the walls, a triangular time-history load distribution, in which the peak value is equal to 110 kN, was applied. The deformation of the studied parapets was recorded in a node located 580 mm above the base and deviated 250 mm from the center.

The static material properties and the rate-dependency issue was addressed for all the formulations; for the macroscopic model in Rafsanjani et al. (2015a), for the mesoscopic model in Rafsanjani et al. (2015b), and for the two-scale model in Silva et al. (2017a). To guarantee the consistency and representativeness of the comparison, the models used the same analytical expressions for the *DIFs*. In particular, the laws made available by Hao and Tarasov (2008), who studied the experimental dynamic behavior of a series of brick and mortar specimens under uniaxial compressive tests through a tri-axial static-dynamic apparatus. As information regarding the strain-rate effects on tensile and shear masonry properties was lacking, the *DIF* regression equations for the tensile and shear material parameters (as the tensile ultimate strength $\sigma_{t0,\mathrm{mortar}}$, mode-I fracture energy G_f^I, cohesion c and mode-II fracture energy G_f^{II}) were assigned to be equal to the compressive ones.

The obtained results are analyzed in terms of displacement magnitude with respect to time. The comparison is achieved through the experimental results (Gilbert et al., 2002) and complemented with a mesoscopic strain-rate independent model by Burnett et al. (2007). Figure 10 shows that the curve from Burnett et al. (2007) leads to excessive displacements (and under stiff response). This author presented a simplified FE mesoscopic model (micro-modeling approach) that represents mortar joints with interface elements. This strategy is strain-rate independent, ergo their accuracy is highly dependent on the static material properties adopted. The use of static strength properties instead of dynamic ones may mislead the results (i.e., an underestimation of the collapse load may occur).

Conversely, the presented numerical models are reasonably accurate in predicting the peak displacement, with a relative error of around 10%. Regarding the post-peak behavior, it is noticeable that the structure displacement restitution of the two-scale model is practically inexistent. Yet, similarly to the experimental results, the latter is not entirely reproduced by the other three numerical models under comparison, presenting both an out-of-plane displacement that slightly decreases in post-peak after the time instant of 180 mm. This is possibly due to the irreversible displacements computed (permanent plastic strains) within the cyclic behavior of the CDP model. The response is still remarkable. The total processing time (CPU time requirements using a laptop with an i7-4710MQ CPU) of the simulations is 0.2 h (12 min) for the two-scale (DNS 3D) model, 2.5 h for the FE macro-model, and 23 h for the FE micro-model.

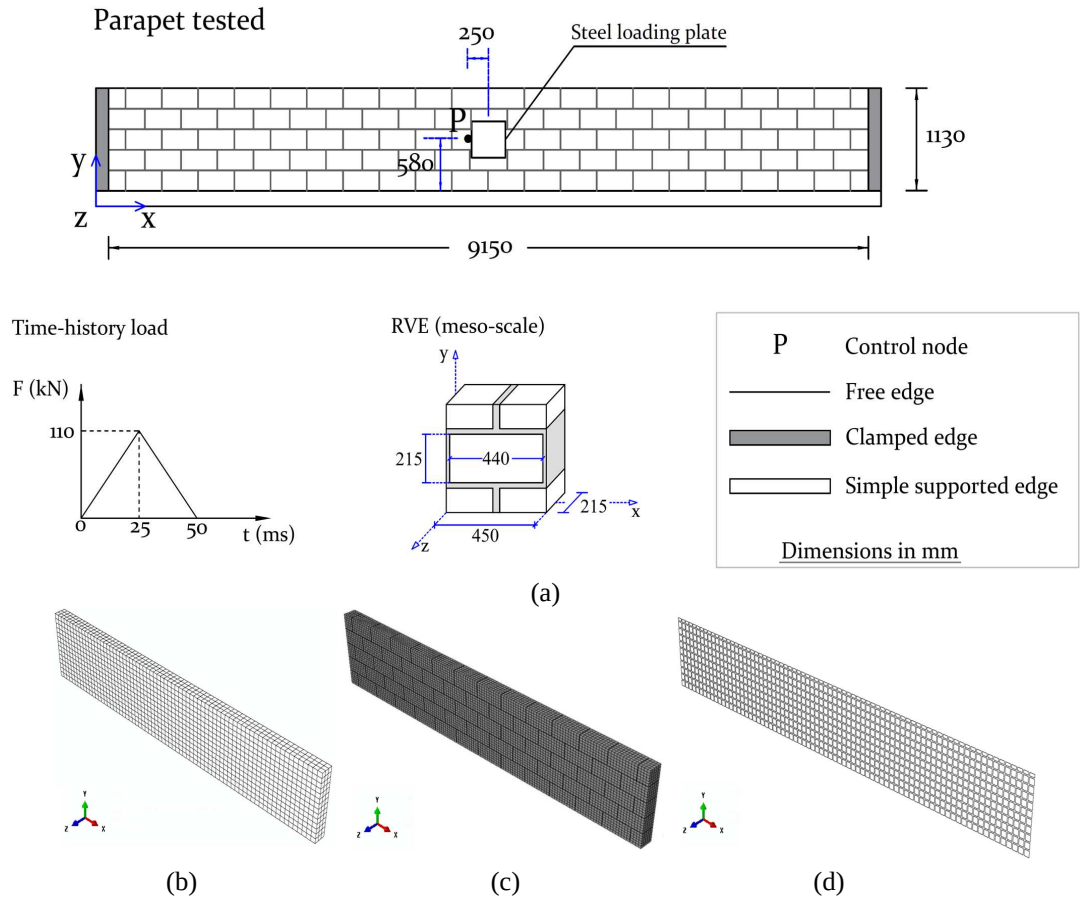

FIG. 9: Sheffield University parapet wall: (a) geometry of the running bond masonry parapets C6 and C7 tested by Gilbert et al. (2002a); and the numerical models presented by the authors that are used in this analysis; (b) the strain-rate FE macroscopic model (macro-model approach); (c) the strain-rate FE mesoscopic model (micro-modeling approach); (d) the strain-rate two-scale homogenized-based model

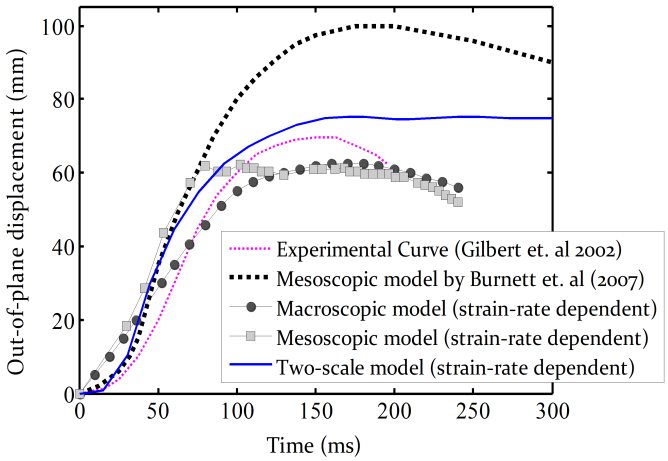

FIG. 10: Time history of the out-of-plane displacement obtained for the control node of the parapets C6 and C7 and deformed shapes observed with the proposed model for the time instants 0.5 ms, 1.41 ms, 25 ms, and 300 ms

4.3 Engineering super Large/Complex Problems: Macro-Scale

4.3.1 Cathedral of the Blessed Sacrament

The Cathedral of the Blessed Sacrament is located in Christchurch city (New Zealand). The building is based on Roman style and was built using Oamaru limestone. The geometrical features are briefly addressed in Figs. 11(a) and 11(b). The building suffered a strengthening intervention in 2004, in which the structural safety level was assumed to be adequate. Yet a sequence of four main seismic events over a period of 9 months, between September 4, 2010 and June 13, 2011, caused progressive damage and local collapse of the two bell towers. Recognizing the symbolism and type of loss associated with this Basilica, a numerical study was conducted to evaluate potential retrofitting strategies that could mitigate the extensive damage found and avoid the collapse of the bell towers. Two strengthening proposals to be implemented in the Cathedral, considering the strengthening intervention of 2004, were analyzed. The goal was to guarantee the ultimate limit state (ULS), that is, to prevent the collapse of structural elements for the highest mean horizontal PGA recorded in the 2010 and 2011 earthquakes. Thus, the value assigned as performance reference for the structural assessment is given by 0.43 g and is defined by the February 2011 seismic event [it corresponds to a period of return around 400 years for new building designs according to the New Zealand Government (2004)].

An FE numerical model was prepared using the presented continuum FE-based anisotropic model (macro-modeling) implemented in the software DIANA (2017). A total-strain fixed crack model was adopted to represent the physical nonlinear behavior. For such a large structure, aiming at reducing the structural global number of degrees of freedom of the Basilica's numerical model, beam, shell and solid finite elements were used. The final FE mesh of the Basilica's model is presented in Fig. 11(c) and corresponds to a total number of 178,719 degrees of freedom. The material and mechanical properties were based on information provided by the NZ authorities and from literature, see Silva et al. (2018) for more details.

The seismic performance of the Cathedral was evaluated through a pushover analysis. This is a time-invariant analysis (static) and is more convenient than a nonlinear dynamic analysis with time integration as it is computational more attractive. A uniform pattern was adopted for the applied horizontal loads, meaning that the distribution of applied forces is proportional to the mass distribution of the structure.

For the first strengthening proposal, a set of 12-meters long stainless-steel tie rods was applied to the structure at the level of the floors being anchored in the slabs. The aim was the improvement of the connection between orthogonal walls, allowing a better force distribution into the nave walls and preventing the out-of-plane collapse of the bell towers. The second strengthening proposal kept the three tie rods of the first proposal at the main façade but includes ring beams at the bell towers instead of the stainless-steel tie rods. Such addition aimed to improve the connection between structural elements, namely the bell towers and nave walls. Furthermore, it allowed better confinement for the bell towers in order to facilitate a better force distribution and prevent out-of-plane collapse.

The efficiency of the strengthening proposals was evaluated based on the pushover analyses for the longitudinal direction – X only [the out-of-plane mechanism of the bell towers and main façade were found Silva et al. (2018) to have the lowest load capacity]. The capacity curves depicted in Fig. 12 shows a clear improvement in the load and

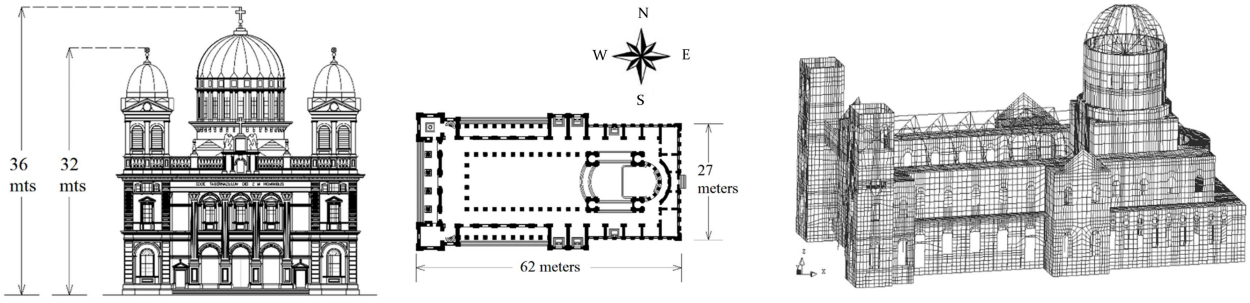

(a) (b) (c)

FIG. 11: Geometry of the Blessed Sacramento Basilica: (a) west elevation; (b) plan; (c) the assumed FE numerical model

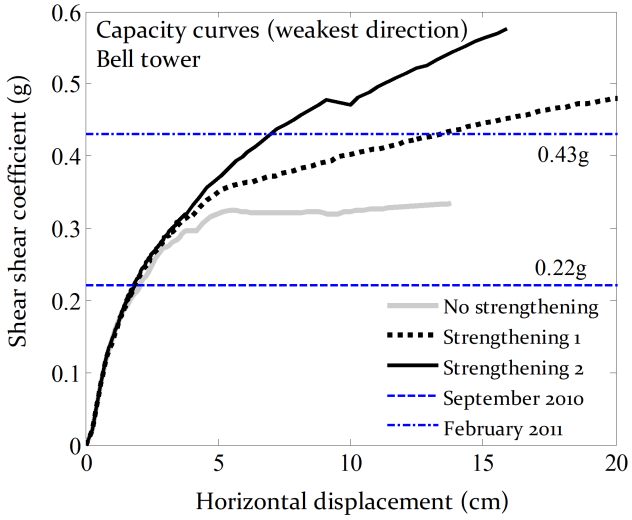

FIG. 12: Obtained capacity curves with and without the strengthening proposals

inelastic displacement capacity of the structure, for which at least a maximum horizontal load of about 0.57 g was obtained (strengthening proposal 2). The first strengthening proposal allows at least a maximum horizontal load equal to 0.49 g. It is noted that the maximum horizontal load applied to the nonstrengthened model is equal to 0.35 g.

The damage assessment was evaluated based on the maximum principal tensile strain, which is a good qualitative indicator of cracking. The structural strengthening undertaken in 2004 played a decisive role in the avoidance of further damage, but this strengthening was insufficient to prevent local failure mechanisms. The crack pattern of the nonstrengthened model shows that the Basilica suffered severe damage in both bell towers and in the vicinity walls for a horizontal load of 0.35 g [Fig. 13(a)]. Extensive cracking due to in-plane shear failure is observed. Figures 13(b) and 13(c) show that the results are in accordance with the intended one, as insignificant damage was observed at the bell tower walls. Hence, the strengthening measures distribute the loads to the nave walls and nave slabs, causing more damage to these elements, namely some cracks on the first floor of the nave.

Finally, the seismic performance of the structure accounting with the strengthening proposals was also evaluated for a horizontal load equal to 0.43 g (PGA of the February 2010 earthquake). Figure 14 presents the principal tensile strains, from which it can be observed that the model with the first strengthening scheme suffered more damage than the one with the second strengthening scheme. Thus, the first strengthening proposal is an effective solution as it creates new load paths and delays failure. However, it does not provide enough strengthening for the two-bell towers in order to change its condition as the most vulnerable elements of the structure. The second strengthening proposal,

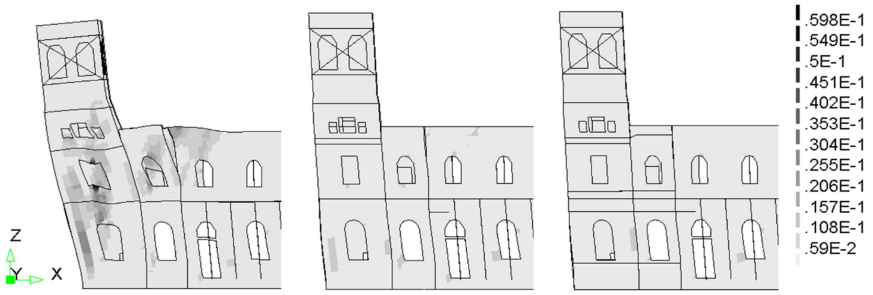

FIG. 13: Comparison of principal tensile strains for the horizontal load equal to 0.35 g: (a) nonstrengthened model; (b) strengthened model 1; (c) strengthened model 2

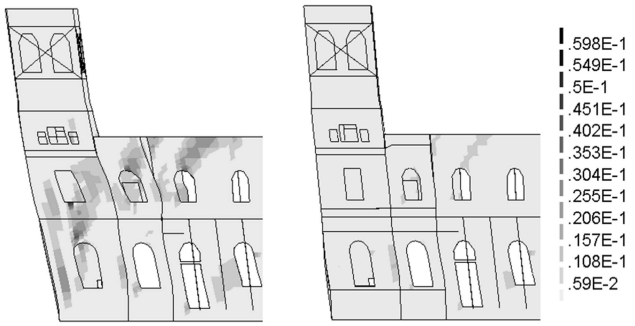

FIG. 14: Comparison of principal tensile strains for the horizontal load equal to 0.43 g: (a) strengthened model 1; (b) strengthened model 2

which includes stainless steel rings, presents the best seismic performance guaranteeing a safety level for the bell towers of at least 40% of the full code requirements (Silva et al., 2018).

The structural strengthening undertaken in 2004 played a decisive role in the avoidance of further damage, but it was insufficient to prevent local failure mechanisms. The numerical results indicate that the structure is unsafe for an earthquake such as the one experienced in February 2011, in which the collapse of the bell towers and significant damage would be expected. The model allowed the identification of two possible strengthening solutions that could change the outcome of similar seismic events to be addressed. The total processing time (CPU time requirements using a laptop with an i7-4710MQ CPU) of the simulations is around 14 h for the nonstrengthened numerical model accounting with the full structure.

4.3.2 Al-Askari Holy Shrine: Blast Load

The Islamic cultural heritage site of Al-Askari Holy Shrine is situated in Samarra, Iraq; its geometry is shown in Fig. 15(a). The Al-Askari shrine suffered a terrorist attack in February 2006. A large quantity of explosive charge (200 kg TNT) had been placed at the top of the dome by taking advantage of the existing scaffold due to the ongoing conservation works (Pandey et al., 2006). The blast load destroyed the dome and the resulting debris damaged the buildings' roof. The majority of the dome's structure collapsed inside the mosque (Baylot and Bevins, 2007). Also, significant damage has been reported in both the East and West façades [Fig. 15(b)].

The continuous anisotropic FE macro-model with strain-rate dependency, presented in Section 3.2, has been used in this study. The main goal is the demonstration of the capability that the proposed advanced numerical tool (meaning the plasticity model) offers in the analysis of full masonry structures under blast load. In this regard, a numerical model featuring the structure of the mosque was developed in ABAQUS (2013). The supports were defined as fixed

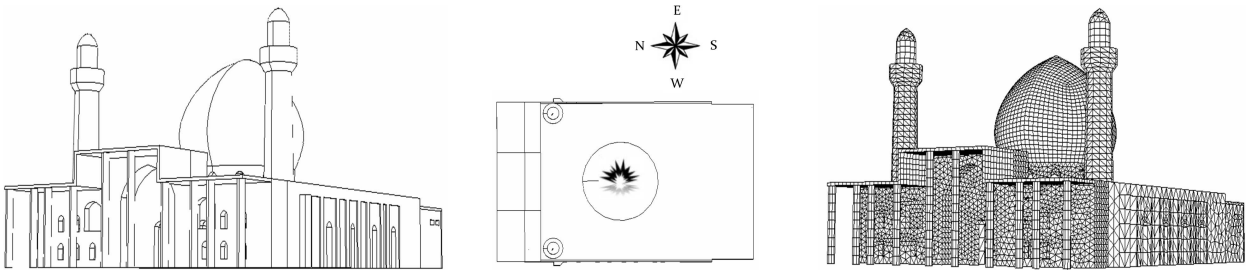

FIG. 15: Islamic cultural heritage site of Al-Askari Holy Shrine: (a) geometry; (b) local where the blast detonation took place (i.e., placed at the top of the dome); (c) FE mesh adopted for the continuum macroscopic model

and only solid FEs were used (i.e., 8-noded linear bricks (reduced integration, hourglass control) and 4-node linear tetrahedron). The final model has a total of 112,623 degrees of freedom and the FE mesh is represented in Fig. 15(c).

The material anisotropy has been considered following adequate literature information, see Rafsanjani (2015). To account with the strain-rate dependency of the masonry composite yield surface, the required DIF laws from the study by Pereira and Lourenço (2016a) have been used. In order to keep the problem with a pure Lagrange formulation, the blast load has been applied as pressure load profiles applied in different zones of the building to assure the representativeness of its distribution. A total of eight zones with different stand-off distances have been modeled. The results of the dynamic analysis are shown next in terms of contour plots for two instant times t.

For a time instant equal to $t = 25$ ms, immediately after the occurrence of the explosion (that occurs for a $t = 20$ ms), the maximum principal plastic strain is given in Fig. 16(a). Significant values are localized in the dome, whereas the incremental deformed shape of Fig. 16(b) shows displacements in the order of 17 cm. The level of loading seems high enough for this structure, hence severe nonlinearity for the masonry behavior and consequently, intense crack formation is reported. Note that the plasticity model does not have incorporated a damage model, yet the plastic strains could be a good qualitative indicator of damage.

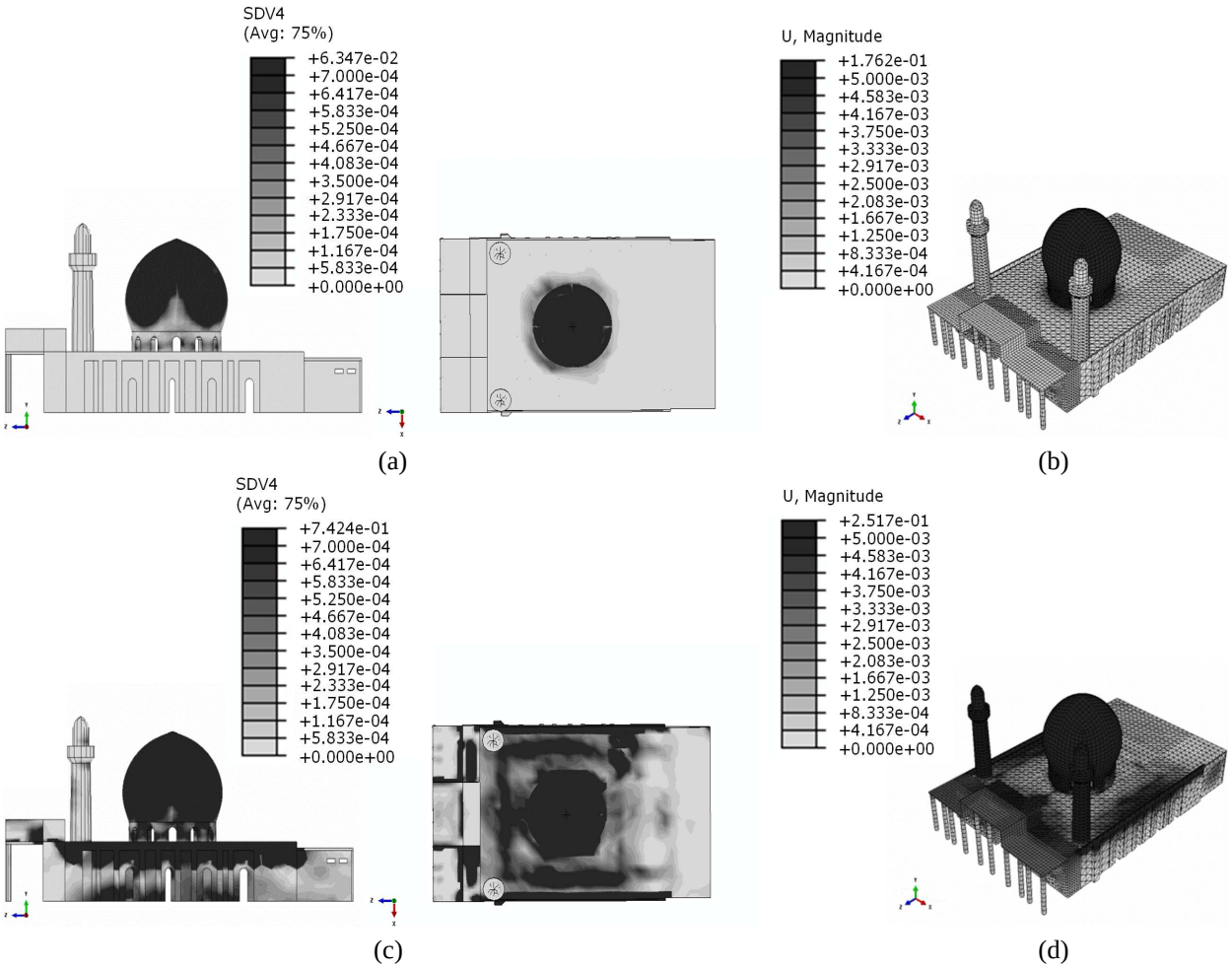

FIG. 16: Results obtained for the Islamic cultural heritage site of Al-Askari after the numerical analysis of a blast load: (a) maximum principal plastic strain after the blast load ($t = 25$ ms); (b) incremental deformed shape (SI unit, m) after the blast load ($t = 25$ ms); (c) maximum principal plastic strain after the most significant over-pressure profiles ($t = 70$ ms); (d) incremental deformed shape (SI unit, m) after the most significant over-pressure profiles ($t = 70$ ms)

The onset of significant damage is visible in the top of the dome but instantly includes its bottom part around the openings. Due to the inertial forces, the dome continues to move during the unloading phase and other parts of the structure, as the roof, minarets, and side facades, are affected. This is addressed in Fig. 16(c), where the maximum principal strain obtained is plotted for $t = 70$ ms (i.e., after the occurrence of the blast and the most significant over-pressures profiles). It is clear now that the damage was more spread in the latter elements, as supported by the incremental deformed shape of Fig. 16(d).

The qualitative evaluation of the damage is presented in detail by Rafsanjani (2015). It has been concluded that the damage pattern found certainly leads to the collapse of the dome and to extensive degradation of both the East and West façades. The addressed conclusions go hand-in-hand with the reported real behavior, ergo proving the adequacy of the advanced strain-rate FE macroscopic model. One may note, however, that the application of the blast load can be a cumbersome task, as demonstrated by other studies (Baylot and Bevins, 2007). The total processing time (CPU time requirements using a laptop with an i7-4710MQ CPU) of the simulation is 101 hours.

5. FINAL REMARKS

FE-based numerical strategies currently have a primary role in the mechanical behavior analysis of masonry structures. Its usefulness is barely questioned, as these are used daily by both the academic and professional communities to solve problems within manageable timelines that otherwise would defy treatment (Linz, 1988). Since computational modeling relies on the physical insight of materials, further developments are continuously needed aiming to decrease the related epistemic and modeling uncertainties.

In such a context, the present article addressed the importance of computational strategies for the numerical analysis of masonry structures. Three advanced FE-based models have been proposed and include an FE micro-model, an FE macro-model, and a novel simplified FE^2 multi-scale model. These models can reproduce the masonry orthotropy, full softening behavior, and loading strain-rate dependency.

The proposed strategies have been used for the engineering of small to large, super-large and complex problems with a focus on the well-known out-of-plane vulnerability of unreinforced masonry structures. The evaluated case studies are the following ones: (i) meso-scale static characterization of the out-of-plane behavior for an English-bond masonry wall; (ii) seismic analysis of the LNEC brick house prototype and the Cathedral of the Blessed Sacrament; (iii) impact load analysis of the Sheffield University parapet wall; and (iv) the blast load analysis of the Al-Askary Holy Shrine.

The small-scale problem included the characterization of the out-of-plane homogenized behavior of an English-bond masonry bond at a meso-scale. The results proved that the mid-thickness vertical joint of an English-bond masonry wall leads to the reduction of its out-of-plane capacity. Reduction of 33% and 17% were found for the horizontal bending and torsional moment peak values, respectively, between a three-dimensional numerical model with and without the discontinuity. This effect has been also witnessed for the large-scale study of the LNEC brick house mock-up. Here, a good agreement between the experimental dynamic response and the one predicted by the simplified multi-scale strategy was found. The FE macro-modeling strategy is, however, unable to capture the lessening of the masonry bending strength and hence to properly predict the structure's behavior when subjected to a seismic load; expected as it assumes an isotropic behavior for the homogeneous equivalent material.

Concerning the complex problem of the Sheffield University parapet wall subjected to an impact load, a good resemble was achieved for all the proposed strategies. A maximum relative error of 10% was found for the out-of-plane displacement of the control node. This error is, however, only achievable since the three proposed models account with the strain-rate dependency of the masonry by dynamic increase factors (DIFs). It has been shown that static material and mechanical properties do not offer adequate insight into the masonry response for fast dynamic problems.

For the super-large and complex problems, as the Cathedral of Blessed Sacrament and the Al-Askari Holy Shrine case studies, the use of an FE macro-model seemed to be the most convenient one as it allows a most straightforward modeling stage. Regarding the former, the numerical model allowed the prediction of the proneness to collapse of the two bell towers of the Cathedral when subjected to the Christchurch seismic events of 2010 and 2011; but, as well, to compare the efficiency of two-retrofitted interventions. Regarding the latter, the FE macro-model allowed to predict

well the collapse of the main dome and capture the severe damage found in both the East and West façades of the Mosque when subjected to a blast load. Although an FE macro-modeling approach is very practical, some attention is recommended when a more detailed description of the response, damage onset, and propagation is desired for a given structural element, as concluded by the obtained smeared damage in the latter problems. In such cases, down-scaling through a micro-modeling or a multi-scale approach could be a proper alternative.

From the conducted analyses, it is noteworthy to address that the modeling strategies adopted for the mechanical study of periodic masonry are mainly dependent on the dimensions of the structure under investigation. For meso-scale problems (order of centimeter), a purely micro-modeling approach seems preferable. Yet, for large or super-large problems (order of meters), as the study of the dynamic behavior of a structural wall or building, the use of a macro-modeling or simplified multi-scale approach is generally followed. In such cases, the potential of a simplified multi-scale model and the inadequacy of an FE micro-model is especially clear for the Sheffield University parapet wall case study. From a computational standpoint, the former is 115 times faster than the FE-micro model and 12.5 times faster than a continuous FE macro-model.

Through a logical extension, a simplified multi-scale approach can significantly decrease the CPU times obtained when using an FE macro-model in the study of super large and complex problems. For instance, the CPU time of 14 hours and 101 hours obtained using an FE macro model for the Cathedral of the Blessed Sacrament and the Al-Askari Holy Shrine Mosque case studies, respectively. It is important to address that the modeling step of such structures using the proposed multi-scale model, through a discrete-based strategy, can be also cumbersome. Hence, the decision of the best strategy should account with the trade-off between the required time for the numerical model preparation and the numerical analysis.

Lastly, the authors stress that the presented FE computational strategies have been implemented in powerful advanced FE software, such as DIANA (2017) and ABAQUS (2013). The latter software is already able to handle parallel computing and thus decrease the required running processing times of the analysis (more evident in large-scale/complex problems). This is an important feature, as it has been seen that the engineering solutions are largely conditioned by the required computational cost associated with the modeling approach followed. Perhaps in a near future, when more powerful computers are of common use (as quantum computers), the engineering of a given problem through a full continuous micro-modeling approach from the meso- to a structural-scale will be, even if contentious from the number of input parameters that demand, feasible from a CPU time standpoint.

ACKNOWLEDGMENTS

This work was partly financed by FEDER funds through the Competitivity Factors Operational Programme – COMPETE and by national funds through FCT – Foundation for Science and Technology within the scope of the project POCI-01-0145-FEDER-007633.

REFERENCES

ABAQUS, Finite Element Analysis (Theory Manual), Release 6.6 (software), Providence: RI: *Dassault Systèmes Simulia Corporation*, 2013.

Adam, J.M., Brencich, A., Hughes, T.G., and Jefferson, T., Micromodelling of Eccentrically Loaded Brickwork: Study of Masonry Wallettes, *Eng. Struct.*, vol. **30**, no. 5, pp. 1244–1251, 2010. DOI: 10.1016/j.engstruct.2009.12.050

Anthoine, A., Derivation of the In-Plane Elastic Characteristics of Masonry through Homogenization Theory, *Int. J. Solids Struct.*, vol. **32**, no. 2, pp. 137–163, 1995. DOI: 10.1016/0020-7683(94)00140-R

Baylot, J.T., Bullock, B., Slawson, T.R., and Woodson, S.C., Blast Response of Lightly Attached Concrete Masonry Unit Walls, *J. Struct. Eng.*, vol. **131**, no. 8, pp. 1186–1193, 2005. DOI: 10.1061/(ASCE)0733-9445(2005)131:8(1186)

Baylot, J.T. and Bevins, T.L., Effect of Responding and Failing Structural Components on the Airblast Pressures and Loads on and inside of the Structure, *Comp. Struct.*, vol. **85**, no. 11, pp. 891–910, 2007. DOI: 10.1016/j.compstruc.2007.01.001

Bažant, Z.P. and Oh, B.H., Crack Band Theory for Fracture of Concrete, *Matériaux Constructions*, vol. **16**, no. 3, pp. 155–177, 1983. DOI: 10.1007/BF02486267

Bažant, Z.P., Xiang, Y., and Prat, P.C., Microplane Model for Concrete. I: Stress-Strain Boundaries and Finite Strain, *J. Eng. Mechan.*, vol. **122**, no. 3, pp. 245–254, 1996. DOI: 10.1061/(ASCE)0733-9399(1996)122:3(245)

Berto, L., Saetta, A., Scotta, R., and Vitaliani, R., An Orthotropic Damage Model for Masonry Structures, *Int. J. Numer. Methods Eng.*, vol. **55**, no. 2, pp. 127–157, 2002. DOI: 10.1002/nme.495

Blanco, P.J., Sánchez, P.J., de Souza Neto, E.A., and Feijóo, R.A., Variational Foundations and Generalized Unified Theory of RVE-Based Multiscale Models, *Arch. Comput. Methods Eng.*, vol. **23**, no. 2, pp. 191–253, 2016. DOI: 10.1007/s11831-014-9137-5

de Borst, R., Remmers, J.J., and Needleman, A., Mesh-Independent Discrete Numerical Representations of Cohesive-Zone Models, *Eng. Fracture Mechan.*, vol. **73**, no. 2, pp. 160–177, 2006. DOI: 10.1016/j.engfracmech.2005.05.007

Buchan, P.A. and Chen, J.F., Blast Resistance of FRP Composites and Polymer Strengthened Concrete and Masonry Structures – A State-of-the-Art Review, *Compos. Part B: Eng.*, vol. **38**, no. 5, pp. 509–522, 2006. DOI: 10.1016/j.compositesb.2006.07.009

De Buhan, P. and De Felice, G., A Homogenisation Approach to the Ultimate Strength of Brick Masonry, *J. Mechan. Phys. Solids*, vol. **45**, no. 7, pp. 1085–1104, 1996. DOI: 10.1016/S0022-5096(97)00002-1

Burnett, S., Gilbert, M., Molyneaux, T., Beattie, G., and Hobbs, B., The Performance of Unreinforced Masonry Walls Subjected to Low-Velocity Impacts: Finite Element Analysis, *Int. J. Impact Eng.*, vol. **34**, no. 8, pp. 1433–1450, 2007. DOI: 10.1016/j.ijimpeng.2006.08.004

Caliò, I., Marletta, M., and Pantò, B., A New Discrete Element Model for the Evaluation of the Seismic Behaviour of Unreinforced Masonry Buildings, *Eng. Struct.*, **40**, pp. 327–338, 2012. DOI: 10.1016/j.engstruct.2012.02.039

Calvi, G.M., Pinho, R., Magenes, G., Bommer, J.J., Restrepo-Vélez, L.F., and Crowley, H., Development of Seismic Vulnerability Assessment Methodologies over the past 30 Years, *ISET J. Earthquake Technol.*, vol. **43**, no. 3, pp. 75–104, 2006.

Candeias, P.X., Campos Costa, A., Mendes, N., Costa, A.A., and Lourenço, P.B., Experimental Assessment of the Out-of-Plane Performance of Masonry Buildings through Shaking Table Tests, *Int. J. Architectural Heritage*, vol. **11**, no. 1, pp. 1–28, 2017. DOI: 10.1080/15583058.2016.1238975

Casolo, S., Rigid Element Model for Non-Linear Analysis of Masonry Façades Subjected to Out-of-Plane Loading, *Commun. Numer. Methods Eng.*, vol. **15**, no. 7, pp. 457–468, 1999.

Casolo, S. and Milani, G., A Simplified Homogenization-Discrete Element Model for the Non-Linear Static Analysis of Masonry Walls Out-of-Plane Loaded, *Eng. Struct.*, vol. **32**, no. 8, pp. 2352–2366, 2010. DOI: 10.1016/j.engstruct.2010.04.010

Casolo, S. and Uva, G., Nonlinear Analysis of Out-of-Plane Masonry Façades: Full Dynamic versus Pushover Methods by Rigid Body and Spring Model, *Earthquake Eng. Struct. Dynam.*, vol. **42**, no. 4, pp. 499–521, 2013. DOI: 10.1002/eqe.2224

Cecchi, A. and Milani, G., A Kinematic FE Limit Analysis Model for Thick English Bond Masonry Walls, *Int. J. Solids Struct.*, vol. **45**, no. 5, pp. 1302–1331, 2008. DOI: 10.1016/j.ijsolstr.2007.09.019

Cecchi, A. and Sab, K., Out of Plane Model for Heterogeneous Periodic Materials: The Case of Masonry, *European J. Mechan.–A/Solids*, vol. **21**, no. 5, pp. 715–746, 2002. DOI: 10.1016/S0997-7538(02)01243-3

Cervera, M. and Chiumenti, M., Mesh Objective Tensile Cracking via a Local Continuum Damage Model and a Crack Tracking Technique, *Comp. Methods Appl. Mechan. Eng.*, vol. **196**, nos. 1-3, pp. 304–20, 2006. DOI: 10.1016/j.cma.2006.04.008

Cundall, P.A. and Hart, P., A Computer Model for Simulating Progressive Large Scale Movements in Blocky Rock Systems, in *Proc. Symp. Rock Fracture (ISRM)*, Nancy, France, vol. **1**, Paper No. II-8, 1971.

D'Ayala, D. and Speranza, E., Definition of Collapse Mechanisms and Seismic Vulnerability of Historic Masonry Buildings, *Earthquake Spectra*, vol. **19**, no. 3, pp. 479–509, 2003. DOI: 10.1193/1.1599896

D'Ayala, D. and Shi, Y., Modeling Masonry Historic Buildings by Multi-Body Dynamics, *Int. J. Architectural Heritage*, vol. **5**, nos. 4-5, pp. 483–512, 2011. DOI: 10.1080/15583058.2011.557138

Dennis, S.T., Baylot, J.T., and Woodson, S.C., Woodson. Response of 1/4-Scale Concrete Masonry Unit (CMU) Walls to Blast, *J. Eng. Mechan.*, vol. **128**, no. 2, pp. 134–142, 2002. DOI: 10.1061/(ASCE)0733-9399(2002)128:2(134)

Dhanasekar, M., Kleeman, P.W., and Page, A.W., The Failure of Brick Masonry under Biaxial Stresses, *Proc. Institut Civil Engineers*, vol. **79**, no. 2, pp. 295–313, 1985. DOI: 10.1680/iicep.1985.992

DIANA, TNO. User's Manual Version 10.2, Delft, The Netherlands. BV, Delft, The Netherlands: *TNO DIANA* 10.2, 2017.

Duvaut, G. and Lions, J.L., *Les Inéquations En Mécanique et En Physique*, P. Dunod, Ed., New York, 1972.

Frankie, T.M., Gencturk, B., and Elnashai, A.S., Simulation-Based Fragility Relationships for Unreinforced Masonry Buildings, *J. Struct. Eng.*, vol. **139**, no. 3, pp. 400–410, 2013. DOI: 10.1061/(ASCE)ST.1943-541X.0000648

Geers, M.G.D., Kouznetsova, V.G., and Brekelmans, W.A.M., Multi-Scale Computational Homogenization: Trends and Challenges, *J. Comput. Appl. Mathemat.*, vol. **234**, no. 7, pp. 2175–2182, 2010. DOI: 10.1016/j.cam.2009.08.077

Georgin, J.F. and Reynouard, J.M., Modeling of Structures Subjected to Impact: Concrete Behaviour under High Strain Rate, *Cement Concrete Compos.*, vol. **25**, no. 1, pp. 131–143, 2003. DOI: 10.1016/S0958-9465(01)00060-9

Giambanco, G., Rizzo, S., and Spallino, R., Numerical Analysis of Masonry Structures via Interface Models, *Comp. Methods Appl. Mechan. Eng.*, vol. **190**, nos. 49-50, pp. 6493–6511, 2001. DOI: 10.1016/S0045-7825(01)00225-0

Gilbert, M., Hobbs, B., and Molyneaux, T.C.K., The Performance of Unreinforced Masonry Walls Subjected to Low-Velocity Impacts: Experiments. *Int. J. Impact Eng.*, vol. **27**, no. 3, pp. 231–251, 2002. DOI: 10.1016/S0734-743X(01)00049-5

Grassl, P. and Jirásek, M., Damage-Plastic Model for Concrete Failure. *Int. J. Solids Struct.*, vol. **43**, no. 22, pp. 7166–7196, 2006. DOI: 10.1016/j.ijsolstr.2006.06.032

Greco, F., Leonetti, L., Luciano, R., and Trovalusci, P., Multiscale Failure Analysis of Periodic Masonry Structures with Traditional and Fiber-Reinforced Mortar Joints, *Compos. Part B: Eng.*, vol. **118**, pp. 75–95, 2017. DOI: 10.1016/j.compositesb.2017.03.004

Griffith, M.C. and Magenes, G., Evaluation of Out-of-Plane Stability of Unreinforced Masonry Walls Subjected to Seismic Excitation, *J. Earthquake Eng.*, vol. **7**, no. 141, pp. 141–169, 2003.

Guragain, R., Worakanchana, K., Mayorca, P., and Meguro, K., Simulation of Brick Masonry Wall Behavior under Cyclic Loading Using Applied Element Method, *JSCE Struct. Eng./Earthquake Eng.*, vol. **58**, no. 6, pp. 531–534, 2006. DOI: 10.11188/seisankenkyu.58.531

Hao, H. and Tarasov, B.G., Experimental Study of Dynamic Material Properties of Clay Brick and Mortar at Different Strain Rates, *Australian J. Struct. Eng.*, vol. **8**, no. 2, p. 117, 2008.

Hao, Y. and Hao, H., Numerical Investigation of the Dynamic Compressive Behaviour of Rock Materials at High Strain Rate, *Rock Mechan. Rock Eng.*, vol. **46**, no. 2, pp. 373–388, 2013. DOI: 10.1007/s00603-012-0268-4

Hao, Y., Hao, H., and Li, Z.X., Influence of End Friction Confinement on Impact Tests of Concrete Material at High Strain Rate, *Int. J. Impact Eng.*, vol. **60**, pp. 82–106, 2013. DOI: 10.1016/j.ijimpeng.2013.04.008

Hendry, E.A.W., Masonry Walls: Materials and Construction, *Construction Building Mater.*, vol. **15**, no. 8, pp. 323–330, 2001. DOI: 10.1016/S0950-0618(01)00019-8

Herbert, D.M., Gardner, D.R., Harbottle, M., and Hughes, T.G., Uniform Lateral Load Capacity of Small-Scale Masonry Wall Panels, *Mater. Struct.*, vol. **47**, no. 5, pp. 805–818, 2014. DOI: 10.1617/s11527-013-0092-7

Hill, R., A Self-Consistent Mechanics of Composite Materials, *J. Mechan. Phys. Solids*, vol. **13**, no. 4, pp. 213–222, 1965. DOI: 10.1016/0022-5096(65)90010-4

Kawai, T., New Discrete Models and Their Application to Seismic Response Analysis of Structures, *Int. J. Nuclear Eng. Design*, vol. **48**, no. 1, pp. 207–229, 1978. DOI: 10.1016/0029-5493(78)90217-0

Konstantinidis, D. and Makris, N., The Dynamics of a Rocking Block in Three Dimensions, *Proc. 8th HSTAM International Congress on Mechanics*, pp. 12–14, 2007.

Lagomarsino, S., Penna, A., Galasco, A., and Cattari, S., TREMURI Program: An Equivalent Frame Model for the Nonlinear Seismic Analysis of Masonry Buildings, *Eng. Struct.*, vol. **56**, pp. 1787–1799, 2013. DOI: 10.1016/j.engstruct.2013.08.002

Lee, J. and Fenves, G.L., Plastic-Damage Model for Cyclic Loading of Concrete Structures, *J. Eng. Mechan.*, vol. **124**, no. 8, pp. 892–900, 1998. DOI: 10.1061/(ASCE)0733-9399(1998)124:8(892)

Lemos, J.V., Discrete Element Modeling of Masonry Structures, *Int. J. Architectural Heritage*, vol. **1**, no. 2, pp. 190–213, 2007. DOI: 10.1080/15583050601176868

Leonetti, L., Trovalusci, P., and Cechi, A., A Multiscale/Multidomain Model for the Failure Analysis of Masonry Walls: A Validation with a Combined FEM/DEM Approach, *Int. J. Multiscale Comput. Eng.*, vol. **16**, no. 4, pp. 325–343, 2018. DOI: 10.1615/IntJMultCompEng.2018026988

Linz, P., A Critique of Numerical Analysis, *Bull. Am. Mathemat. Soc.*, vol. **19**, pp. 407–416, 1998. DOI: 10.1090/S0273-0979-1988-15682-0

Lotfi, H.R. and Shing, P.B., Interface Model Applied to Fracture of Masonry Structures, *J. Struct. Eng.*, vol. **120**, no. 1, pp. 63–80, 1994. DOI: 10.1061/(ASCE)0733-9445(1994)120:1(63)

Lourenço, P.B., Computational Strategies for Masonry Structures, PhD, Delft University of Technology, Delft, The Netherlands, 1996.

Lourenço, P.B., An Anisotropic Macro-Model for Masonry Plates and Shells: Implementation and Validation, TNO Building and Construction Research – Computational Mechanics, Report no. 03.21.1.31.07, pp. 34–91, 1997.

Lourenço, P.B., Anisotropic Softening Model for Masonry Plates and Shells, *J. Struct. Eng.*, vol. **126**, no. 9, pp. 1008–1016, 2000. DOI: 10.1061/(ASCE)0733-9445(2000)126:9(1008)

Lourenço, P.B., Recent Advances in Masonry Structures: Micromodelling and Homogenisation, in *Multiscale Modeling in Solid Mechanics, Computational and Experimental Methods in Structures*, Imperial College Press, vol. **3**, pp. 251–294, 2009. DOI: 10.1142/p604

Lourenço, P.B., De Borst, R., and Rots, J.G., A Plane Stress Softening Plasticity Model for Orthotropic Materials, *Int. J. Numer. Methods Eng.*, vol. **40**, no. 21, pp. 4033–4057, 1997. DOI: 10.1002/(SICI)1097-0207(19971115)40:21<4033::AID-NME248>3.0.CO;2-0

Lourenço, P.B. and Rots, J.G., Multisurface Interface Model for Analysis of Masonry Structures, *J. Eng. Mechan.*, vol. **123**, no. 7, pp. 660–668, 1997. DOI: 10.1061/(ASCE)0733-9399(1997)123:7(660)

Lubliner, J., Oliver, J., Oller, S., and Oñate, E., A Plastic-Damage Model for Concrete, *Int. J. Solids Struct.*, vol. **25**, no. 3, pp. 299–326, 1989. DOI: 10.1016/0020-7683(89)90050-4

Macorini, L. and Izzuddin, B.A., A Non-Linear Interface Element for 3D Mesoscale Analysis of Brick-Masonry Structures, *Int. J. Numer. Methods Eng.*, vol. **85**, no. 12, pp. 1584–1608, 2011. DOI: 10.1002/nme.3046

Macorini, L. and Izzuddin, B.A., Nonlinear Analysis of Unreinforced Masonry Walls under Blast Loading Using Mesoscale Partitioned Modeling, *J. Struct. Eng.*, vol. **140**, no. 8, 2014. DOI: 10.1061/(ASCE)ST.1943-541X.0000931

Macorini, L. and Izzuddin, B.A., Nonlinear Analysis of Masonry Structures Using Mesoscale Partitioned Modelling, *Adv. Eng. Software*, vols. **60**–**61**, pp. 58–69, 2013. DOI: 10.1016/j.advengsoft.2012.11.008

Malomo, D., Pinho, R., and Penna, A., Using the Applied Element Method for Modelling Calcium Silicate Brick Masonry Subjected to In-Plane Cyclic Loading, *Earthquake Eng. Struct. Dynam.*, vol. **47**, no. 7, pp. 1610–1630, 2018. DOI: 10.1002/eqe.3032

Meguro, K. and Tagel-Din, H., Applied Element Method for Structural Analysis: Theory and Application for Linear Materials, *JSCE Struct. Eng./Earthquake Eng.*, vol. **17**, no. 1, pp. 21–35, 2000.

Milani, G., Lourenço, P.B., and Tralli, A., Homogenised Limit Analysis of Masonry Walls, Part II: Structural Examples, *Comp. Struct.*, vol. **84**, nos. 3-4, pp. 181–195, 2006. DOI: 10.1016/j.compstruc.2005.09.004

Milani, G., 3D Upper Bound Limit Analysis of Multi-Leaf Masonry Walls, *Int. J. Mechan. Sci.*, vol. **50**, no. 4, pp. 817–836, 2008. DOI: 10.1016/j.ijmecsci.2007.11.003

Milani, G., Lourenço, P.B., and Tralli, A., Homogenization Approach for the Limit Analysis of Out-of-Plane Loaded Masonry Walls, *J. Struct. Eng.*, vol. **132**, no. 10, pp. 1650–1663, 2006. DOI: 10.1061/(ASCE)0733-9445(2006)132:10(1650)

Milani, G. and Tralli, A., Simple SQP Approach for Out-of-Plane Loaded Homogenized Brickwork Panels, Accounting for Softening, *Comp. Struct.*, vol. **89**, nos. 1-2, pp. 201–215, 2011. DOI: 10.1016/j.compstruc.2010.09.005

Nard, H.L. and Bailly, P., Dynamic Behaviour of Concrete: The Structural Effects on Compressive Strength Increase, *Mechan. Cohesive-Frictional Mater.*, vol. **5**, no. 6, pp. 491–510, 2000. DOI: 10.1002/1099-1484(200008)5:6<491::AID-CFM106>3.0.CO;2-R

New Zealand Government, NZS 1170.5: 2004 Structural Design Actions – Part 5: Earthquake Design Actions – New Zealand, 2004.

Otero, F., Oller, S., Martinez, X., and Salomón, O., Numerical Homogenization for Composite Materials Analysis. Comparison with Other Micro Mechanical Formulations, *Compos. Struct.*, vol. **122**, pp. 405–416, 2015. DOI: 10.1016/j.compstruct.2014.11.041

Pandey, A.K., Kumar, R., Paul, D.K., and Trikha, D.N., Non-Linear Response of Reinforced Concrete Containment Structure under Blast Loading, *Nuclear Eng. Design*, vol. **236**, no. 9, pp. 993–1002, 2006. DOI: 10.1016/j.nucengdes.2005.09.015

Pantò, B., Cannizzaro, F., Caliò, I., and Lourenço, P.B., Numerical and Experimental Validation of a 3D Macro-Model for the In-Plane and Out-of-Plane Behavior of Unreinforced Masonry Walls, *Int. J. Architectural Heritage*, vol. **11**, no. 7, pp. 946–964, 2017. DOI: 10.1080/15583058.2017.1325539

Pau, A. and Trovalusci, P., Block Masonry as Equivalent Micropolar Continua: The Role of Relative Rotations, *Acta Mechanica*, vol. **223**, no. 7, pp. 1455–1471, 2012. DOI: 10.1007/s00707-012-0662-8

Pereira, J.M., Campos, J., and Lourenço, P.B., Masonry Infill Walls under Blast Loading Using Confined Underwater Blast Wave Generators (WBWG), *Eng. Struct.*, vol. **92**, pp. 69–83, 2015. DOI: 10.1016/j.engstruct.2015.02.036

Pereira, J.M. and Lourenço, P.B., Experimental Characterization of Masonry and Masonry Components at High Strain Rates, *J. Mater. Civil Eng.*, vol. **29**, no. 2, 2016a. DOI: 10.1061/(ASCE)MT.1943-5533.0001755

Pereira, J.M. and Lourenço, P.B., Experimental Bond Behaviour of GFRP and Masonry Bricks under Impulsive Loading, *Mater. Struct.*, vol. **49**, no. 11, pp. 4799–4811, 2016b. DOI: 10.1617/s11527-016-0826-4

Petracca, M., Pelà, L., Rossi, R., Oller, S., Camata, G., and Spacone, E., Regularization of First Order Computational Homogenization for Multiscale Analysis of Masonry Structures, *Comput. Mechan.*, vol. **57**, no. 2, pp. 257–276, 2016. DOI: 10.1007/s00466-015-1230-6

Pontiroli, C., Rouquand, A., and Mazars, J., Predicting Concrete Behaviour from Quasi-Static Loading to Hypervelocity Impact, *European J. Environ. Civil Eng.*, vol. **14**, nos. 6-7, pp. 703–727, 2010. DOI: 10.1080/19648189.2010.9693259

Quagliarini, E., Maracchini, G., and Clementi, F., Uses and Limits of the Equivalent Frame Model on Existing Unreinforced Masonry Buildings for Assessing Their Seismic Risk: A Review, *J. Building Eng.*, vol. **10**, pp. 166–182, 2017. DOI: 10.1016/j.jobe.2017.03.004

Rafsanjani, S.H., Lourenço, P.B., and Peixinho, N., Implementation and Validation of a Strain Rate Dependent Anisotropic Continuum Model for Masonry, *Int. J. Mechan. Sci.*, vol. **104**, pp. 24–43, 2015a. DOI: 10.1016/j.ijmecsci.2015.10.001

Rafsanjani, S.H., Lourenço, P.B., and Peixinho, N., Dynamic Interface Model for Masonry Walls Subjected to High Strain Rate Out-of-Plane Loads, *Int. J. Impact Eng.*, vol. **76**, pp. 28–37, 2015b. DOI: 10.1016/j.ijimpeng.2014.09.002

Rafsanjani, S., High Strain Rate Constitutive Modeling for Historical Structures Subjected to Blast Loading, PhD, University of Minho, from http://hdl.handle.net/1822/38459, 2015.

Reccia, E., Leonetti, L., Trovalusci, P., and Cecchi, A., A Multiscale/Multidomain Model for the Failure Analysis of Masonry Walls: A Validation with a Combined FEM/DEM Approach, *Int. J. Multiscale Comput. Eng.*, **16**, no. 4, pp. 325–343, 2018. DOI: 10.1615/IntJMultCompEng.2018026988

Roca, P., Cervera, M., and Gariup, G., Structural Analysis of Masonry Historical Constructions. Classical and Advanced Approaches, *Arch. Comput. Methods Eng.*, vol. **17**, no. 3, pp. 299–325, 2010. DOI: 10.1007/s11831-010-9046-1

Roca, P., Cervera, M., Pelà, L., Clemente, R., and Chiumenti, M., Continuum FE Models for the Analysis of Mallorca Cathedral, *Eng. Struct.*, vol. **46**, pp. 653–670, 2013. DOI: 10.1016/j.engstruct.2012.08.005

Rots, J.G., Nauta, P., Kusters, G., and Blaauwendraad, J., Smeared Crack Approach and Fracture Localization in Concrete, *Heran*, vol. **30**, pp. 1–47, 1985.

Sarhosis, V., Tsavdaridis, K.D., and Giannopoulos, I., Discrete Element Modelling (DEM) for Masonry Infilled Steel Frames with Multiple Window Openings Subjected to Lateral Load Variations, *Open Construct. Building Technol. J.*, vol. **8**, no. 1, pp. 93–103, 2014. DOI: 10.2174/1874836801408010093

Sejnoha, J., Sejnoha, M., Zeman, J., Sykora, J., and Vorel, J., A Mesoscopic Study on Historic Masonry, *Struct. Eng. Mechan.*, vol. **30**, no. 1, pp. 99–117, 2008. DOI: 10.12989/sem.2008.30.1.099

Silva, L.C., Lourenço, P.B., and Milani, G., Rigid Block and Spring Homogenized Model (HRBSM) for Masonry Subjected to Impact and Blast Loading, *Int. J. Impact Eng.*, vol. **109**, pp. 14–28, 2017a. DOI: 10.1016/j.ijimpeng.2017.05.012

Silva, L.C., Lourenço, P.B., and Milani, G., Nonlinear Discrete Homogenized Model for Out-of-Plane Loaded Masonry Walls, *J. Struct. Eng.*, vol. **143**, no. 9, p. 4017099, 2017b. DOI: 10.1061/(ASCE)ST.1943-541X.0001831

Silva, L.C., Lourenço, P.B., and Milani, G., Derivation of the Out-of-Plane Behaviour of Masonry through Homogenization Strategies: Micro-Scale Level, *Comp. Struct.*, vol. **209**, pp. 30–43, 2018. DOI: 10.1016/j.compstruc.2018.08.013

Silva, L.C., Mendes, N., Lourenço, P.B., and Ingham, J., Seismic Structural Assessment of the Christchurch Catholic Basilica, New Zealand, *Structures*, vol. **15**, pp. 115–130, 2018. DOI: 10.1016/j.istruc.2018.06.004

Sinha, B.P., A Simplified Ultimate Load Analysis of Laterally-Loaded Model Orthotropic Brickwork Panels of Low Tensile Strength, *Struct. Eng. ASCE*, vol. **56B**, no. 4, pp. 81–84, 1978.

Sluys, L.J. and De Borst, R., Computational Modeling of Impact Tests on Steel Fibre Reinforced Concrete Beams, *Heron*, vol. **37**, no. 4, pp. 3–15, 1992.

Spahn, J., Andrä, H., Kabel, M., and Müller, R., A Multiscale Approach for Modeling Progressive Damage of Composite Materials Using Fast Fourier Transforms, *Comp. Methods Appl. Mechan. Eng.*, vol. **268**, pp. 871–883, 2014. DOI: 10.1016/j.cma.2013.10.017

Taliercio, A., Closed-Form Expressions for the Macroscopic in-Plane Elastic and Creep Coefficients of Brick Masonry, *Int. J. Solids Struct.*, vol. **51**, no. 17, pp. 2949–2963, 2014. DOI: 10.1016/j.ijsolstr.2014.04.019

Theodossopoulos, D. and Sinha, B., A Review of Analytical Methods in the Current Design Processes and Assessment of Performance of Masonry Structures, *Construct. Building Mater.*, vol. **41**, pp. 990–1001, 2013. DOI: 10.1016/j.conbuildmat.2012.07.095

Tomaževič, M., *Earthquake-Resistant Design of Masonry Buildings*, vol. **1**, World Scientific, 1999.

Trovalusci, P., Ostoja-Starzewski, M., De Bellis, M.L., and Murrali, A., Scale-Dependent Homogenization of Random Composites as Micropolar Continua, *European J. Mechan.–A/Solids*, vol. **49**, pp. 396–407, 2015. DOI: 10.1016/j.euromechsol.2014.08.010

Wu, C., Hao, H., and Lu, Y., Dynamic Response and Damage Analysis of Masonry Structures and Masonry Infilled RC Frames to Blast Ground Motion, *Eng. Struct.*, vol. **27**, no. 3, pp. 323–333, 2005. DOI: 10.1016/j.engstruct.2004.10.004

Zapata, B.J., and Weggel, D., Collapse Study of an Unreinforced Masonry Bearing Wall Building Subjected to Internal Blast Loading, *J. Performance Constructed Facilities*, vol. **22**, no. 2, pp. 92–100, 2008. DOI: 10.1061/(ASCE)0887-3828(2008)22:2(92)

Zucchini, A. and Lourenço, P.B., A Micro-Mechanical Model for the Homogenisation of Masonry, *Int. J. Solids Struct.*, vol. **39**, no. 12, pp. 3233–3255, 2002. DOI: 10.1016/S0020-7683(02)00230-5